

1052

ANALYSIS OF THE STRESS STATE IN AN IOSIPESCU SHEAR TEST SPECIMEN



David E. Walrath
Donald F. Adams

June 1983

{NASA-CR-176745) ANALYSIS OF THE STRESS STATE IN AN IOSIPESCU SHEARTEST SPECIMEN	N86-24755
Technical Report, May 1982 - May 1983	
{Wyoming Univ.) 86 p HC A05/MF A01 CSCL 11D	Unclas
	G3/24 42911

TECHNICAL REPORT

NASA-Langley Research Center
Grant No. NAG-1-272

COMPOSITE MATERIALS RESEARCH GROUP
MECHANICAL ENGINEERING DEPARTMENT
UNIVERSITY OF WYOMING
LARAMIE, WYOMING 82071

Approved for Public Release: Distribution Unlimited

COMPOSITE MATERIALS RESEARCH GROUP
DEPARTMENT of MECHANICAL ENGINEERING
University of Wyoming Laramie, Wyoming 82071

1 Report No.	2 Government Accession No.	3 Recipient's Catalog No.	
4 Title and Subtitle Analysis of the Stress State in an Iosipescu Shear Test Specimen		5 Report Date June 1983	
		6 Performing Organization Code	
7 Author(s) David E. Walrath Donald F. Adams		8 Performing Organization Report No. UWME-DR-301-102-1	
		10 Work Unit No.	
9 Performing Organization Name and Address Composite Materials Research Group University of Wyoming Laramie, Wyoming 82071		11 Contract or Grant No. NAG-1-272	
		13 Type of Report and Period Covered Technical Report May 1982-May 1983	
12 Sponsoring Agency Name and Address NASA-Langley Research Center Hampton, Virginia 23665		14 Sponsoring Agency Code	
		15 Supplementary Notes	
18 Abstract The state of stress in an Iosipescu shear test specimen is analyzed, utilizing a finite element computer program. The influence of test fixture configuration on this stress state is included. Variations of the standard specimen configuration, including notch depth, notch angle, and notch root radius are modeled. The purpose is to establish guidelines for a specimen geometry which will accommodate highly orthotropic materials while minimizing stress distribution nonuniformities. Materials ranging from isotropic to highly orthotropic are considered. An optimum specimen configuration is suggested, along with changes in the test fixture.			
17 Key Words (Suggested by Author(s)) Composite Materials Test Methods Shear Testing Finite Element Analysis		18 Distribution Statement Unclassified, Unlimited	
19 Security Classif. (of this report) Unclassified	20 Security Classif. (of this page) Unclassified	21 No. of Pages 84	22 Price*

* For sale by the National Technical Information Service, Springfield, Virginia 22161

DEPARTMENT REPORT
UWME-DR-301-102-1

ANALYSIS OF THE STRESS STATE IN
AN IOSIPESCU SHEAR TEST SPECIMEN

DAVID E. WALRATH
DONALD F. ADAMS

JUNE 1983

TECHNICAL REPORT

NASA-LANGLEY RESEARCH CENTER
GRANT NO. NAG-1-272

COMPOSITE MATERIALS RESEARCH GROUP
MECHANICAL ENGINEERING DEPARTMENT
UNIVERSITY OF WYOMING
LARAMIE, WYOMING 82071

APPROVED FOR PUBLIC RELEASE: DISTRIBUTION UNLIMITED

1. Report No.	2. Government Accession No.	3. Recipient's Catalog No.	
4. Title and Subtitle Analysis of the Stress State in an Iosipescu Shear Test Specimen		5. Report Date June 1983	
		6. Performing Organization Code	
7. Author(s) David E. Walrath Donald F. Adams		8. Performing Organization Report No. UWME-DR-301-102-1	
		10. Work Unit No.	
9. Performing Organization Name and Address Composite Materials Research Group University of Wyoming Laramie, Wyoming 82071		11. Contract or Grant No. NAG-1-272	
		13. Type of Report and Period Covered Technical Report May 1982-May 1983	
12. Sponsoring Agency Name and Address NASA-Langley Research Center Hampton, Virginia 23665		14. Sponsoring Agency Code	
		15. Supplementary Notes	
18. Abstract The state of stress in an Iosipescu shear test specimen is analyzed, utilizing a finite element computer program. The influence of test fixture configuration on this stress state is included. Variations of the standard specimen configuration, including notch depth, notch angle, and notch root radius are modeled. The purpose is to establish guidelines for a specimen geometry which will accommodate highly orthotropic materials while minimizing stress distribution nonuniformities. Materials ranging from isotropic to highly orthotropic are considered. An optimum specimen configuration is suggested, along with changes in the test fixture.			
17. Key Words (Suggested by Author(s)) Composite Materials Test Methods Shear Testing Finite Element Analysis		18. Distribution Statement Unclassified, Unlimited	
19. Security Classif. (of this report) Unclassified	20. Security Classif. (of this page) Unclassified	21. No. of Pages 84	22. Price*

* For sale by the National Technical Information Service, Springfield, Virginia 22161

PREFACE

This final report presents results of an analytical study performed for the National Aeronautics and Space Administration-Langley Research Center under Grant Number NAG-1-272. Mr. Marvin B. Dow served as the NASA-Langley Program Monitor.

All work under this program was performed by members of the Composite Materials Research Group (CMRG) within the Department of Mechanical Engineering at the University of Wyoming. The head of CMRG is Dr. Donald F. Adams, Professor of Mechanical Engineering. Mr. David E. Walrath, CMRG Staff Engineer, served as Principal Investigator for this program. Mr. Robert F. Cilensek, Graduate Student in Mechanical Engineering, performed much of the detailed numerical analysis. Also assisting during the program were Mr. Merrill A. Bishop and Mr. Dennis K. McCarthy, Undergraduate Students in Mechanical Engineering.

TABLE OF CONTENTS

	<u>Page</u>
SECTION 1. INTRODUCTION AND SUMMARY	1
1.1 Introduction	1
1.2 Summary	4
SECTION 2. DESCRIPTION OF THE CURRENT TEST METHOD	5
2.1 Test Fixture	5
2.2 Test Specimens	7
2.3 Shear Strain Measurement	10
SECTION 3. ANALYTICAL TECHNIQUE AND RESULTS	15
3.1 Model Description	15
3.2 Problem Variations	17
3.3 Analysis of the Present Test Geometry	17
3.3.1 Isotropic Material ($E_{11}/E_{22} = 1.0$)	19
3.3.2 Orthotropic Material ($E_{11}/E_{22} = 13.3$)	25
3.3.3 Highly Orthotropic Material ($E_{11}/E_{22} = 49.4$)	40
3.3.4 Summary	45
3.4 Effect of Notch Depth	45
3.5 Effect of Notch Angle	51
3.6 Effect of Notch Tip Radius	60
3.7 Optimum Specimen Geometry	65
SECTION 4. TEST FIXTURE IMPROVEMENTS	73
4.1 Weakness of the Current Test Fixture	73
4.2 Redesigned Test Fixture	74
SECTION 5. DISCUSSION	77
REFERENCES	81

SECTION 1

INTRODUCTION AND SUMMARY

1.1 Introduction

At the present time, there is a recognized need for an accurate, simple, and inexpensive test method for measuring the shear properties of anisotropic materials, particularly fiber-reinforced composite materials. Many methods have been used to measure shear properties of various composite materials, including thin-walled tube [1,2] and solid rod [3] torsion tests, the off-axis tensile test [4-7], picture frame and rail shear tests [8-12], the cross-sandwich beam test [13-15], the slotted tension shear test [16], the plate-twist test [17,18], the short beam shear test [19], the split ring shear test [20], and others. While all of these tests have some utility in certain specific applications, none meet all of the criteria of being simple to perform, generally applicable to any material, and capable of measuring both shear strength and shear modulus.

A shear test method which does meet the above three criteria was first suggested by Nicolae Iosipescu of Bucharest, Rumania in the early 1960's. He published his test method extensively, as shown by the list of Rumanian language papers referenced in his 1967 English language paper [21]. Since most of his work was published in Rumanian, however, it attracted little attention outside of his own country. Iosipescu was primarily interested in testing isotropic metals, not anisotropic composite materials.

The Iosipescu shear test method has been extensively used within the Composite Materials Research Group (CMRG) at the University of

Wyoming for more than five years. During this time period, many hundreds of specimens of a wide variety of composite materials have been tested, including three-dimensionally reinforced carbon-carbon composites [22, 23], unidirectionally-reinforced graphite/epoxy [24, 25] and glass/epoxy [26], glass fiber-reinforced polyester sheet molding compounds [27-29], and even materials such as wood and foam [26]. Tests described in the above references have included both static and fatigue loadings, and have also involved both in-plane and through-the-thickness shear loadings. A description of the Iosipescu shear test method as used at the University of Wyoming, as well as a summary of typical test results, have been recently published in References [27,30].

Based upon Iosipescu's original work [21], several modified versions of the test method have evolved. Slepetz, et al. [31] utilized a slightly modified loading scheme, and termed the test the Asymmetrical Four-Point Bending (AFPB) test. While this modification permits easier specimen loading, the induced shear stress becomes a function of the loading point location dimensions, a distinct disadvantage in comparison to the Iosipescu configuration, as discussed in detail in Reference [29]. Slepetz, et al., did do a very thorough study, however, including an investigation of stress uniformity using strain gages, Moiré interferometry, and a finite element analysis. The latter was also used to study the influence of specimen notch geometry.

Another variation, intended primarily as a method of inducing a general biaxial stress state in a composite plate, but useful also as a shear test method, is that utilized by Arcan, et al. [32-35]. The test specimen is a circular disk with cutouts, resulting in a small test zone in the central region. In the practical sense, this test method, when

used with unidirectional composites oriented in the principal directions of the fixture, corresponds to the Iosipescu shear test.

An excellent finite element analysis of the test configuration utilized by Arcan, et al. [32-35] has been presented by Marloff [36].

The Iosipescu shear test method has also been subjected to finite element analyses by several investigators. In addition to the work of Slepetz, et al. [31] previously referred to, other investigators have also performed detailed studies [37,38], using a two-dimensional, linearly elastic analysis. The specimen was modeled as bonded to stiff end fixtures, loaded in tension. Thus, one concern, not present in the Iosipescu test method as used by the present investigators, was the influence on stress distributions of the bonded tabs. These investigators also studied the influence of rounding the notch tips. Their general conclusion was that the Iosipescu specimen does produce a region of reasonably uniform shear stress at the center of the specimen, for both isotropic (as demonstrated by Iosipescu [21] originally) and orthotropic materials [37]. Any nonuniformity of the shear stress between the notch tips was found to be highly dependent upon the elastic properties of the orthotropic material, being most pronounced for unidirectional composites. The complex state of stress present at the sharp notch tips for these orthotropic materials was considered to contribute to failure, hence their interest in rounding the notch tips.

In Reference [38], the authors concluded that the double V-notched (i.e., the Iosipescu) shear specimen is worthy of further investigation, both numerically and experimentally. No experimental work was performed in References [37,38].

1.2 Summary

During this present first-year effort, the Iosipescu shear test specimen was analyzed using the finite element method to determine the stress state within the specimen. Nine different notch geometries were modeled, including variations in notch depth, notch angle, and notch tip radius. These different geometries were analyzed using material properties with orthotropy ratios (E_{11}/E_{22}) ranging from 1 (isotropic aluminum) to a highly orthotropic ($E_{11}/E_{22} = 49.4$) GY70/904 unidirectional graphite/epoxy. During this program, several modifications to the test method which produce a more uniform shear stress state within the test specimen were established. Specifically, these include using a different notch angle and notch tip radius than established by Iosipescu for isotropic materials. Additionally, the test fixture itself should be redesigned to slightly shift the loading point locations. During this redesign, other modifications to the test fixture can be incorporated to simplify its use, thus making the test procedure more efficient.

SECTION 2

DESCRIPTION OF THE CURRENT TEST METHOD

2.1 Test Fixture

The Iosipescu shear test achieves a state of pure shear loading within the test section of the specimen, by application of two counteracting moments produced by two force couples. The force, shear, and moment diagrams based on simple mechanics of materials analysis of beams for this test method are shown in Figure 1. For a total force P , as measured at the testing machine load cell, the forces applied to the test specimen are as shown in Figure 1a, based on equilibrium requirements. The distance "a" is measured between forces of the outermost force couple and "b" is the distance between forces of the innermost force couple. A state of constant shear loading is induced in the center section of the test specimen, as illustrated in Figure 1b. This shearing force is equal in magnitude to the applied load P . As can be seen in Figure 1c, the induced moment at the center of the specimen is zero; the two induced moments exactly cancel at that point. Therefore, the loading state is pure shear loading at the specimen midlength. The notches in the test specimen shift the shear stress distribution from parabolic to uniform, as will be discussed later in this section.

A means by which such a loading may be achieved is shown in Figure 2. Each end of the test specimen is restrained from rotating by the loading fixture, while at the same time undergoing shear loading as the right fixture half moves relative to the left half.

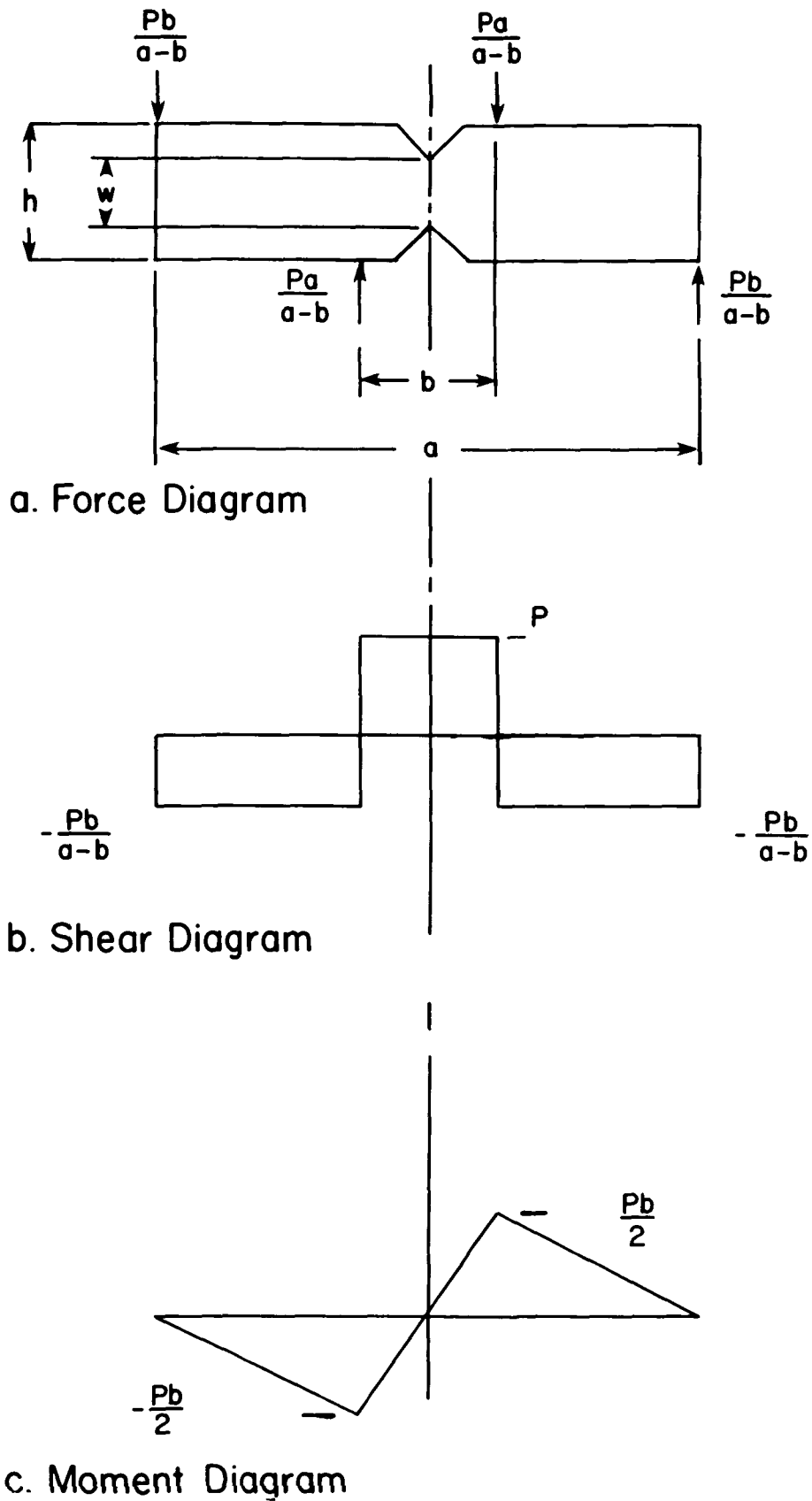


Figure 1. Force, Shear, and Moment Diagrams for the Iosipescu Shear Test Method.

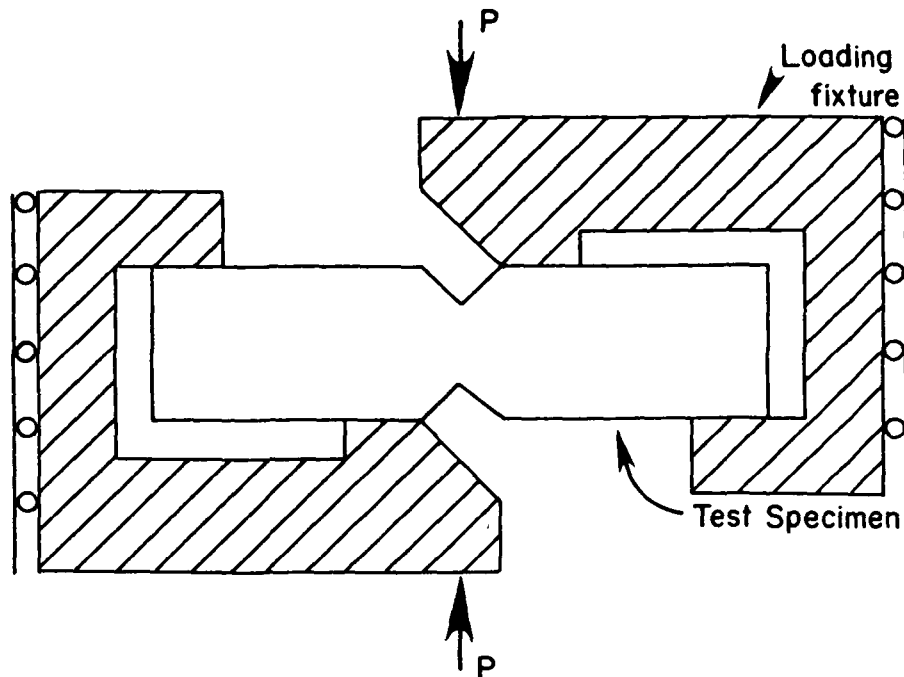


Figure 2. Schematic of the Loading Fixture for an Iosipescu Shear Test

The actual test fixture used for performing Iosipescu shear tests at Wyoming is shown in Figure 3. An example test specimen of clear acrylic plastic is shown in place within the fixture. The steel piece extending above the test fixture behind the ball is a removable alignment tool used for centering the specimen by indexing on the upper notch. Compressive force is applied to the steel ball loading point, resulting in downward motion of the right half of the test fixture, which slides on a 1.9 cm (0.75 in) diameter steel post. Several limitations exist with this current fixture design. These will be discussed in a later section along with proposed fixture improvements.

2.2 Test Specimens

The test specimens used in the fixture shown in Figure 3 are 51 mm (2 in) long, 12.7 mm (0.5 in) wide and of arbitrary "as received" material thickness, as shown in Figure 4. The fixture shown will

ORIGINAL PAGE IS
OF POOR QUALITY

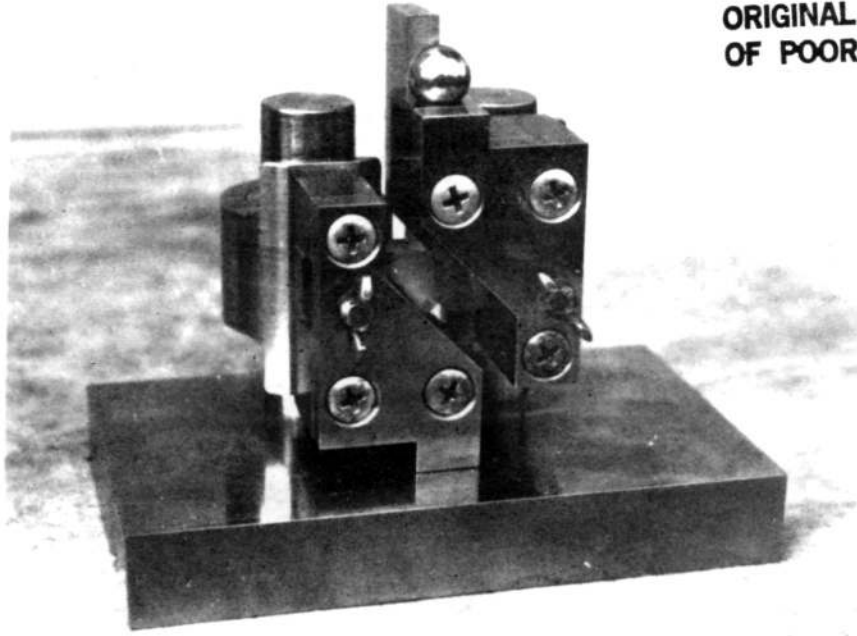


Figure 3. Iosipescu Shear Test Fixture

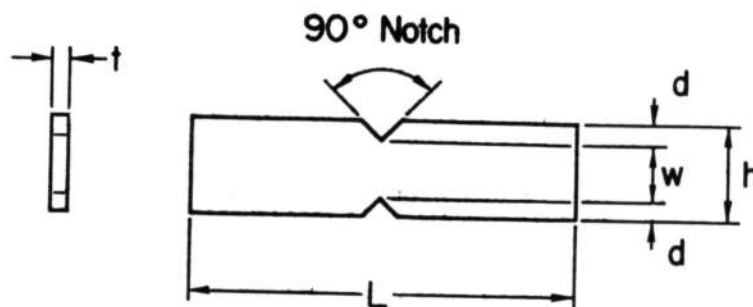


Figure 4. Iosipescu Shear Test Specimen

t = "as received"
w = 7.62 mm (0.3 in)
d = 2.54 mm (0.1 in)
L = 50.8 mm (2.0 in)

accommodate material up to 12.7 mm (0.5 in) thick. A 90° included angle notch is cut into each edge of the specimen at the midlength to a depth of 2.5 mm (0.1 in). Iosipescu established that by cutting 90° notches on each edge of the test specimen, the shear stress distribution within an isotropic test specimen could be altered from the parabolic shear stress distribution present in constant cross section beams to a uniform shear stress distribution in the region between the notches. Contrary to intuitive expectations, no tensile or compressive stress concentrations are caused by these notches, at least for isotropic materials. Iosipescu argued that the stress concentration did not occur because the sides of the notches are parallel to the normal stress directions at that point in the test specimen [21]. Therefore, the shear stress obtained using the Iosipescu method is simply the applied force P divided by the net cross-sectional area between the two notch tips. The purpose of the present investigation was to analytically study the effect of notch size and geometry on the shear stress distribution, while looking for possible stress concentration effects.

The thickness of the test specimen shown in Figure 4 should, in general, be on the order of 2.5 mm (0.1) or greater to avoid compression buckling-induced failures. It is possible to test very thin materials by bonding multiple layers together to increase the specimen thickness, or by using reinforcing tabs in the loading regions [26]. The maximum thickness is arbitrary, within practical limits. The fixture shown in Figure 3 will accommodate a specimen up to 12.7 mm (0.5 in) thick.

With reference to any given set of material coordinate axes, six shear stress components can be defined. For present purposes, the 1- and 2- axes are defined as the in-plane coordinate axes. The 3-axis is

then in the out-of-plane direction, i.e., in the through-the-thickness direction. For orthotropic materials, the 1-direction is taken to correspond to the primary material direction. Conventional double subscript shear stress notation is used, with the shear stress acting on a plane perpendicular to the first coordinate direction, parallel to the second direction. Therefore, in-plane shear tests are defined as 12 or 21 tests, while through-the-thickness shear tests are denoted 13, 31, 23, or 32. It is theoretically possible to use the Iosipescu shear test to measure shear properties for any of the six possible shear components. This is done by laminating materials to the desired length or width, as is shown in Figures 5b and 5c. As is discussed in References [27,30], all possible orientations of the shear test have been performed at Wyoming; however, we do not recommend use of the specimen shown in Figure 5b. This configuration is fragile and therefore very susceptible to damage. Through-the-thickness shear properties can be measured more easily and accurately with the test specimen of Figure 5c. Marloff [36] also noted problems in testing unidirectional graphite fiber-reinforced composites when the fibers were oriented in the vertical direction, i.e., in a 21 test orientation. Again, it is recommended that when testing orthotropic materials, the 1 direction should be aligned with the long axis of the test specimen.

2.3 Shear Strain Measurement

The current technique for measuring shear strain in the Iosipescu shear test is with strain gages. Strain gages oriented at $\pm 45^\circ$ to the longitudinal axis of the test specimen are bonded at the specimen midlength, as shown in Figure 6. The analytical results to be presented in Section 3 show that this measurement technique works well. However,

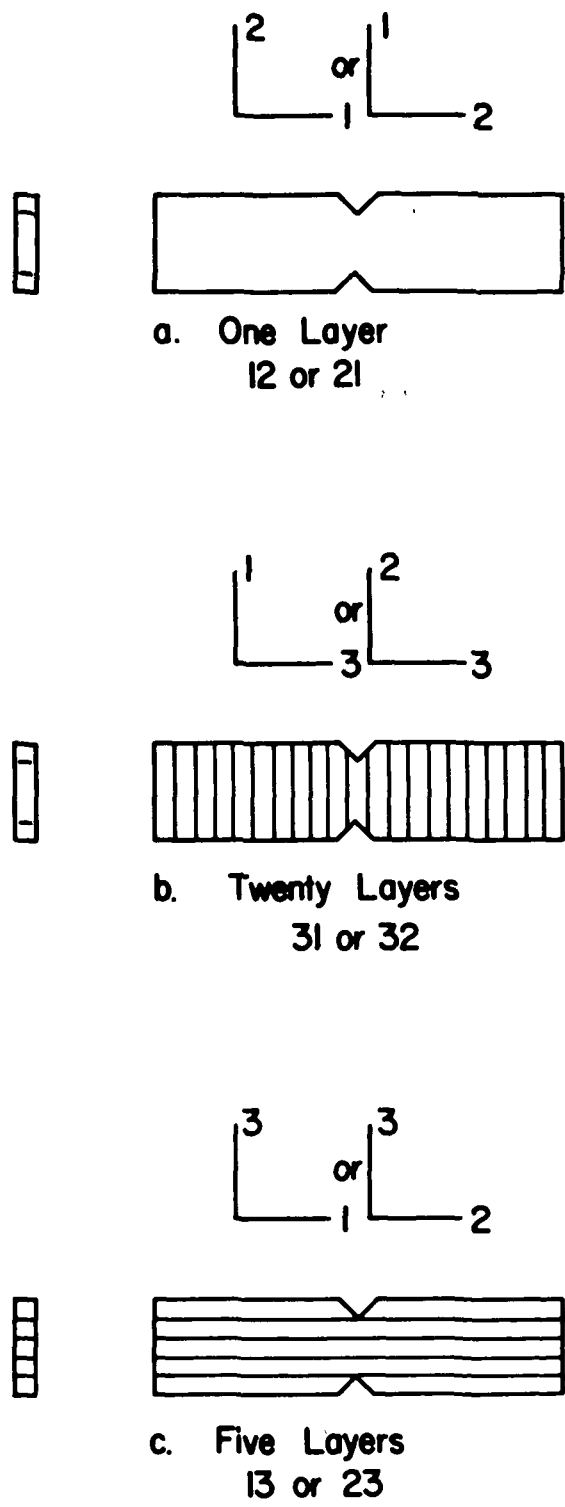


Figure 5. Iosipescu Shear Test Specimen Configurations
Assuming $t = 2.5 \text{ mm}$ (0.1 in)

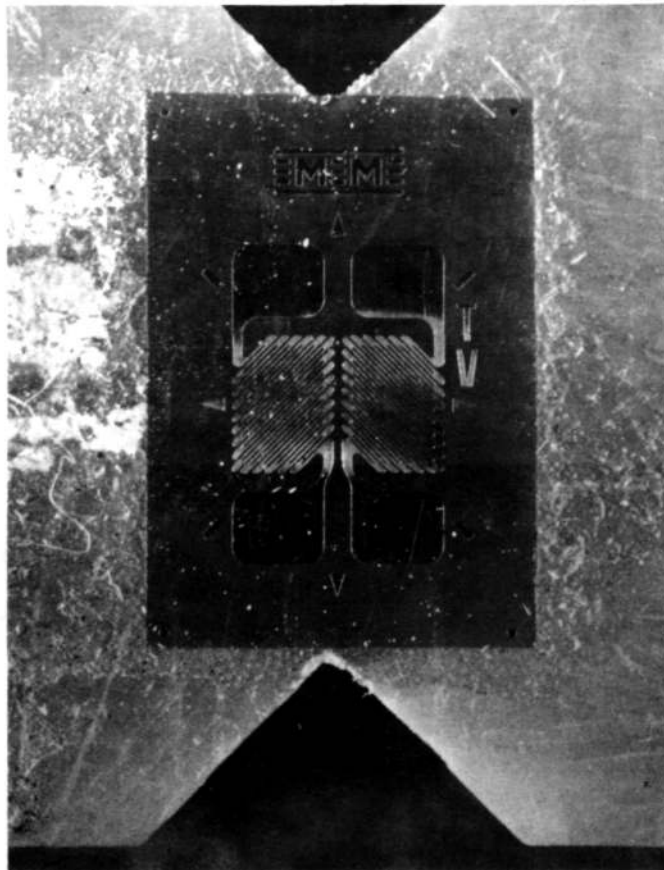


Figure 6. Strain Gages Mounted on an Iosipescu Shear Test Specimen

problems have been encountered in testing fiber-reinforced polymers at elevated temperature and elevated humidity. Also, conventional foil strain gages do not possess sufficient range to measure the full shear strain to failure for materials which deform nonlinearly in shear, e.g., elevated temperature tests of polymers.

A modified extensometer in place of strain gages has been used at Wyoming to measure shear strains. This transducer attaches along two lines parallel to the shear loading direction, to measure the relative shear displacement, as shown in Figure 7. This technique has been at least partially successful, warranting further study. Improving shear strain measuring capability will be one task undertaken during the planned second-year study.

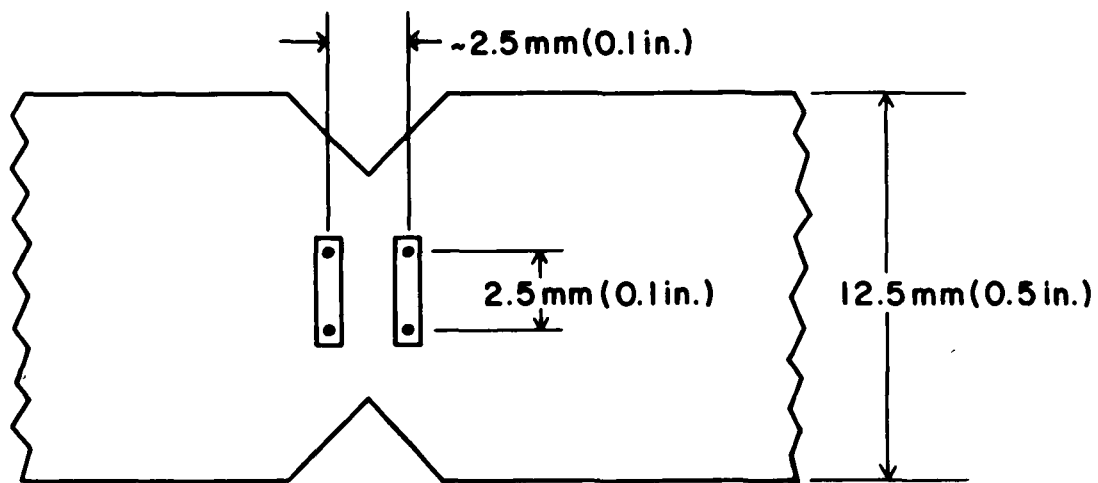


Figure 7. Shear Strain Transducer Attachment Points for the Iosipescu Shear Test

SECTION 3

ANALYTICAL TECHNIQUE AND RESULTS

3.1 Model Description

This program was initiated with the intention of doing a full three-dimensional orthotropic, elastoplastic finite element analysis of the Iosipescu shear specimen. For this reason, the models to be presented in this report were formulated using 8-node three-dimensional brick elements. As a first analytical look at the problem, however, only one layer of elements was used, making the results presented here effectively two-dimensional. These preliminary results indicated a number of interesting trends, which were therefore pursued in terms of geometry and material variations. Thus, the full three-dimensional analysis of a composite laminate has not yet been completed. This study of laminated Iosipescu shear specimens will be completed during the second-year effort, and presented in a subsequent report.

The baseline model used to study the Iosipescu shear specimen is shown in Figure 8. The model consists of 590 nodes and 256 eight-node isoparametric elements. The analysis was conducted assuming six degrees of freedom per node, i.e., three displacements and three rotations. Because the Iosipescu specimen geometry problem is asymmetric (see Figures 1 and 2), it was necessary to model the entire specimen in the x-y plane. A plane of symmetry does exist parallel to the x-y plane through the center of the specimen thickness; therefore, only half of the specimen need be modeled in the z-direction.

Loading was applied by prescribing displacement boundary conditions as shown in Figure 9. This simulates the rigid test fixture shown in

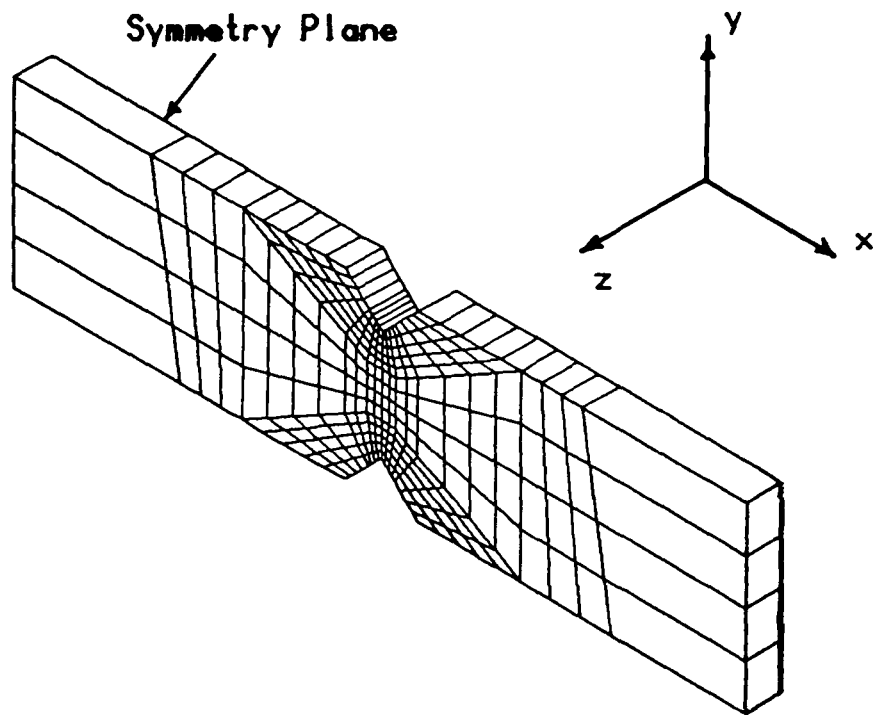


Figure 8. Iosipescu Shear Specimen Finite Element Grid

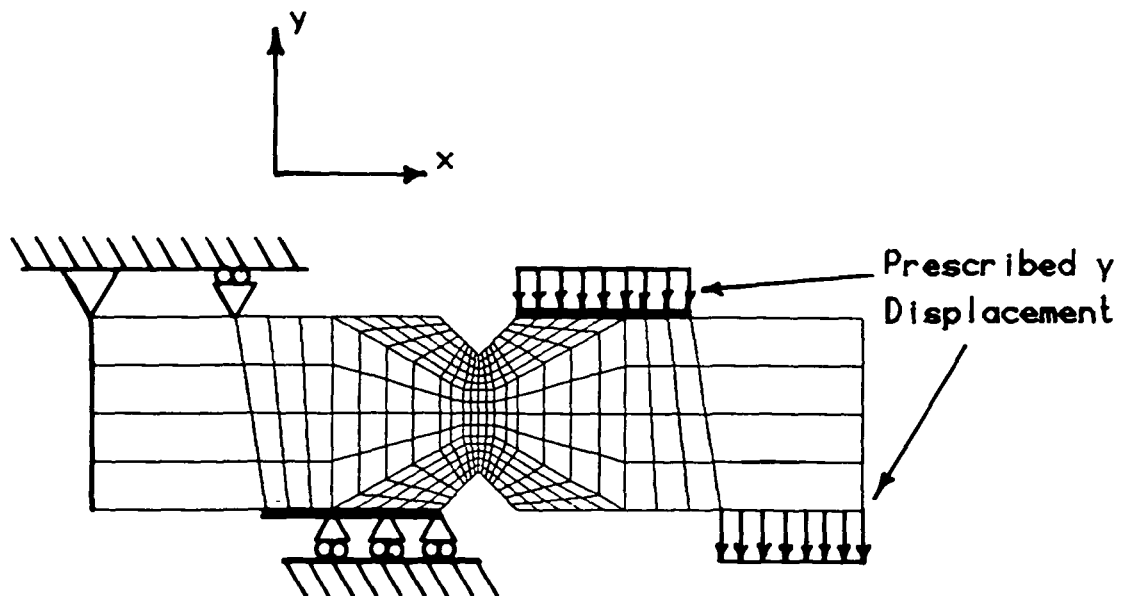


Figure 9. Boundary Conditions Used in Modeling the Iosipescu Shear Specimen

Figures 2 and 3. Note, this presumes no rotation of the specimen within the test fixture. To obtain the required symmetry in the z direction, all nodes on the back face of the test specimen (see Figure 8) were constrained in the z direction.

3.2 Problem Variations

The major region of interest in this analysis was the notch region. Consequently, most of the problem variations were related to notch geometry. The effects of different notch depths and different notch tip radii were studied. In addition, different notch angles were examined. Finally, the applicability of the Iosipescu shear test to different materials was also studied. The various geometric variations were analyzed using material properties ranging from isotropic to highly orthotropic. A matrix of the possible computer runs which could be performed is presented in Table 1. As can be seen from the problem matrix of Table 1, there are 81 possible computer runs. In actuality, it was necessary to run only 25 of these cases as some of the geometry combinations proved to be unacceptable test geometries.

Input material properties for the three materials used are shown in Table 2. The composite materials were presumed to be transversely isotropic. Note that there are three degrees of orthotropy, with E_{11}/E_{22} ratios ranging from 1.0 (isotropic) to a highly orthotropic E_{11}/E_{22} ratio of 49.4. The optimum test geometry was analyzed for all three sets of material properties.

3.3 Analysis of the Present Test Geometry

The current test specimen configuration was discussed in Section 2. It is 50.8 mm (2 in) long and 12.7 mm (0.5 in) wide. The notches are 90° included angle, each cut to a depth equal to 20 percent of the

Table 1
Iosipescu Shear Specimen Analysis Variations

Property	Variations Considered		
Material Orthotropy Ratio, E_{11}/E_{22}	1.0 (aluminum)	13.3 (AS/3501-6 graphite/epoxy)	49.4 (GX70/904 graphite/epoxy)
Notch Depth (percent of width)	10	20	30
Notch Tip (mm) Radius (in)	0.000 0.000	0.625 0.025	1.290 0.050
Notch Angle (degrees)	90	110	120

Table 2
Input Material Properties Assumed

<u>2024-T4 Aluminum Alloy [39,40]</u>		<u>$E_{11}/E_{22} = 1$</u>
$E_{11} = E_{22} = E_{33}$	73.1 GPa	(10.6 Msi)
$\nu_{12} = \nu_{13} = \nu_{23}$	0.33	
$G_{12} = G_{13} = G_{23}$	$E/2(1+\nu_{12})$	
<u>AS/3501-6 Graphite Epoxy [41]</u>		<u>$E_{11}/E_{22} = 13.3$</u>
E_{11}	138 GPa	(20.0 Msi)
$E_{22} = E_{33}$	10.3 GPa	(1.5 Msi)
$\nu_{12} = \nu_{13}$	0.28	
ν_{23}	0.25	
$G_{12} = G_{13}$	5.52 GPa	(0.8 Msi)
G_{23}	$E_{22}/2(1+\nu_{23})$	
<u>GX70/904 Graphite/Epoxy [41]</u>		<u>$E_{11}/E_{22} = 49.4$</u>
E_{11}	303 GPa	(44.0 Msi)
$E_{22} = E_{33}$	6.1 GPa	(0.89 Msi)
$\nu_{12} = \nu_{13}$	0.25	
ν_{23}	0.25	
$G_{12} = G_{13}$	4.14 GPa	(0.60 Msi)
G_{23}	$E_{22}/2(1+\nu_{23})$	

width, i.e., to a depth of 2.5 mm (0.1 in). The notch radius is very small, assumed to be zero in the analysis. The finite element grid for this geometry is shown in Figure 8.

3.3.1 Isotropic Material ($E_{11}/E_{22} = 1.0$)

Normalized stress contour plots for an isotropic (aluminum) material are presented in Figures 10 through 12. Contour values have been normalized by the absolute value of the average applied shear stress, $\bar{\tau}$, as calculated from the reaction forces at the loaded boundaries. Thus, the average applied shear stress is defined as the total applied load divided by the cross-sectional area between the notch tips. Normalizing by dividing by the absolute value of the applied shear stress preserves the algebraic signs of the contour values. Therefore, positive normal stresses are tensile and negative stresses are compressive. Note that for this test configuration and defined coordinate system, the actual applied shear stress τ is negative.

Looking first at Figure 10, it can be seen that the normalized longitudinal (bending) stresses, $\sigma_x/|\bar{\tau}|$, at the center of the test specimen are very low, as the 0.00 contours denoted by the letter "G" are the only contours present. Bending stresses do increase with increasing horizontal distance from the vertical centerline of the specimen, particularly near the notch tip, as illustrated by the F and H contour lines. However, there is not a large σ_x stress concentration due to the presence of the notch, just as Iosipescu originally stated [21]. Normalized transverse (vertical) normal stress contours $\sigma_y/|\bar{\tau}|$, are plotted in Figure 11. Again it will be noted that the center of the test region between the notch tips is relatively stress-free. However, significant compressive stresses are present to the right of the upper

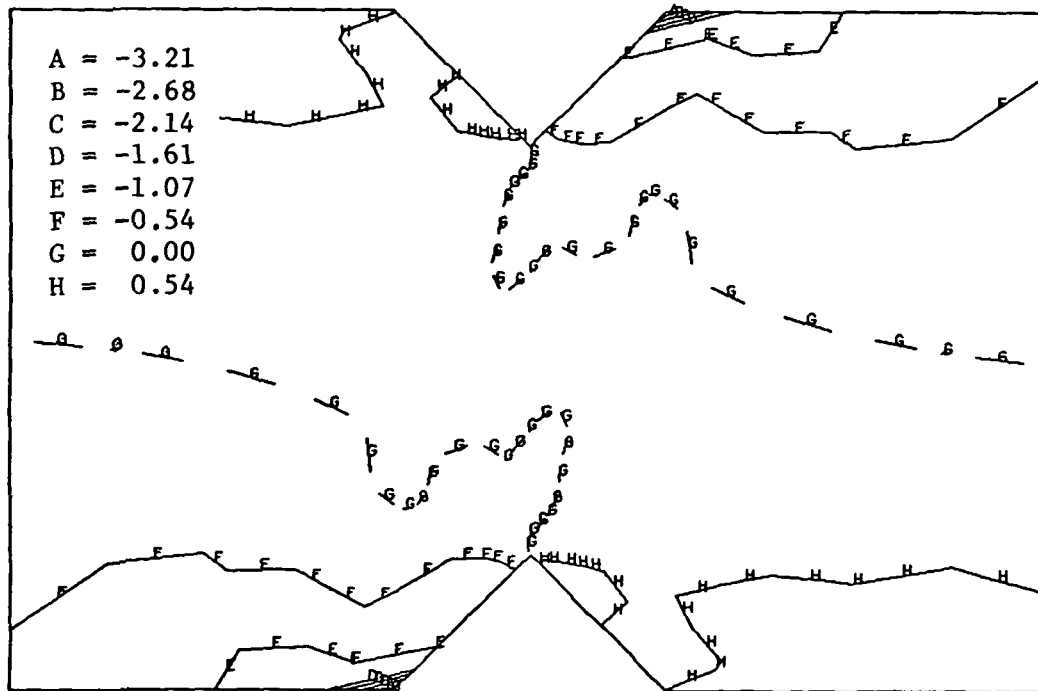


Figure 10. Normalized Longitudinal (Bending) Stress Contours $\sigma_x/|\bar{\tau}|$ for an Orthotropy Ratio of 1.0.

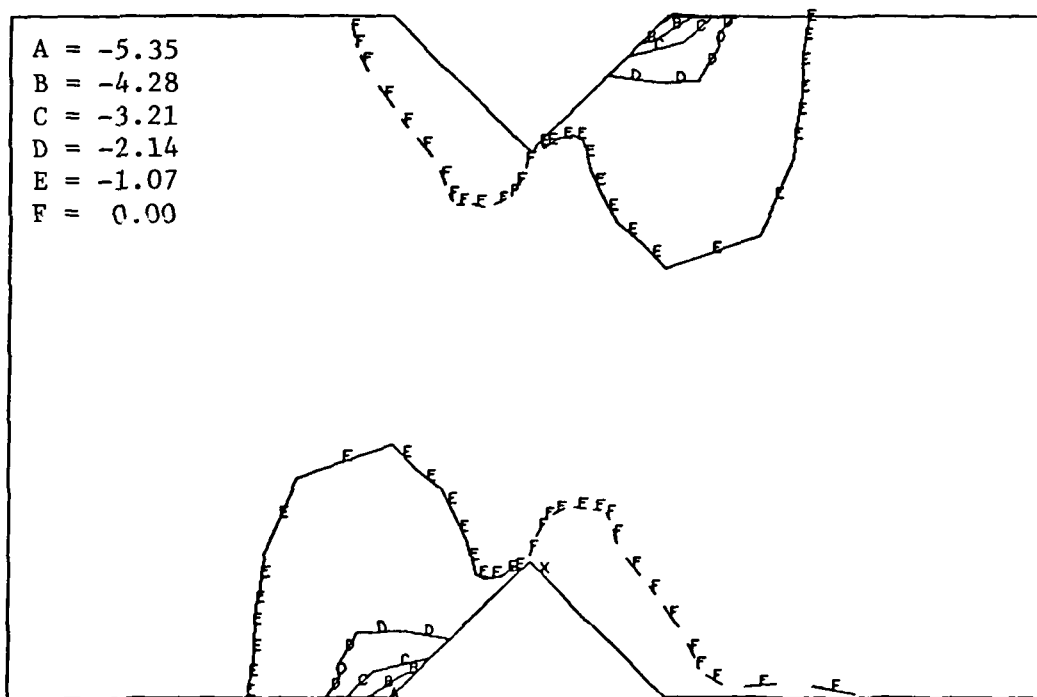


Figure 11. Normalized Transverse Normal Stress Contours $\sigma_y/|\bar{\tau}|$ for an Orthotropy Ratio of 1.0.

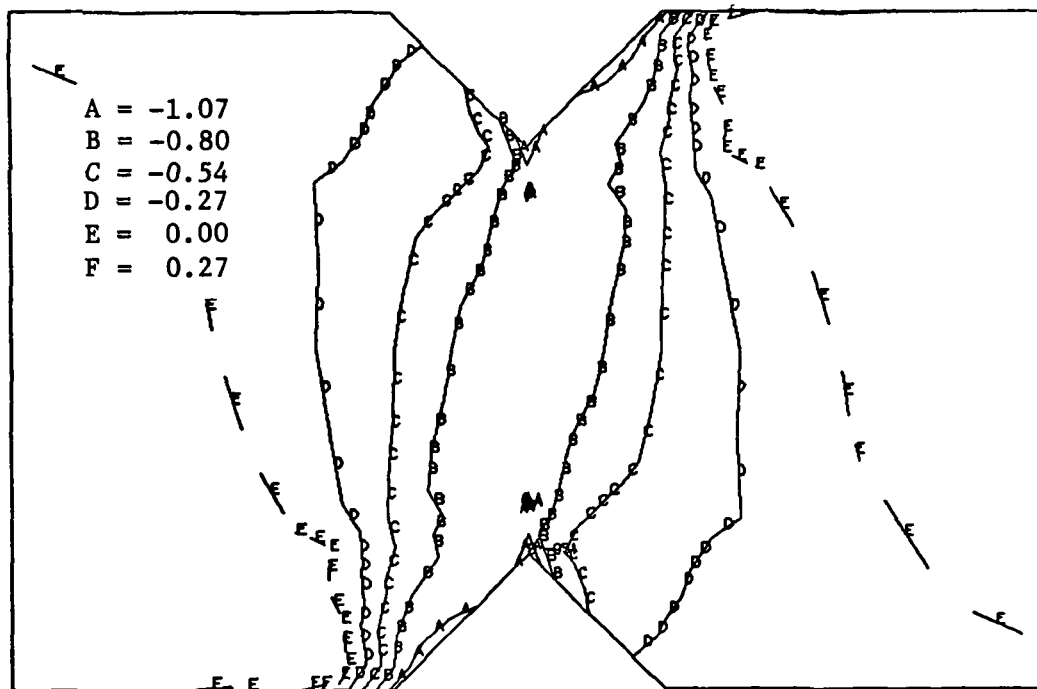


Figure 12. Normalized Shear Stress Contours $\tau_{xy}/|\bar{\tau}|$ for an Orthotropy Ratio of 1.0.

notch, and to the left of the lower notch, due to the fixture loadings being applied at these points. The normalized reaction force profile for the upper center loading point is plotted in Figure 13. Forces were normalized by dividing by the total applied load. Note how rapidly these stresses rise approaching the edge of the notch. The influence of these loading-induced compressive stresses extends into the test region of the specimen. This points out an obvious flaw in the current test configuration. The center loading surfaces need to be moved away from the notches in the specimen.

Normalized (in-plane) shear stress contours $\tau_{xy}/|\bar{\tau}|$ are plotted in Figure 12. This plot demonstrates that the shear stress distribution within the region between the notches is reasonably uniform. The normalized shear stress contour values range from -0.8 to -1.1 (it will be recalled that this test configuration produces negative shear stresses). The maximum normalized shear stress value is 1.3, occurring at the tip of the notch. These results seem to indicate a shear stress concentration effect caused by the notch. A similar result has been previously noted by Herakovich and Bergner [38], who used a much more refined finite element mesh in this region. One objective of this present analytical study is to minimize this shear stress concentration without producing other stress profile irregularities.

A plot of the normalized shear stress distribution at the specimen centerline is shown in Figure 14. In this plot and similar shear stress distribution plots to be subsequently presented, the normalizing value is $\bar{\tau}$ rather than $|\bar{\tau}|$, to dispense with the negative sign on shear stress. Again it will be noted that the shear stress distribution is fairly uniform, rising as the notch tip is approached.

BOUNDARY NODAL FORCE DISTRIBUTION

$$E_{11}/E_{22} = 1.0$$

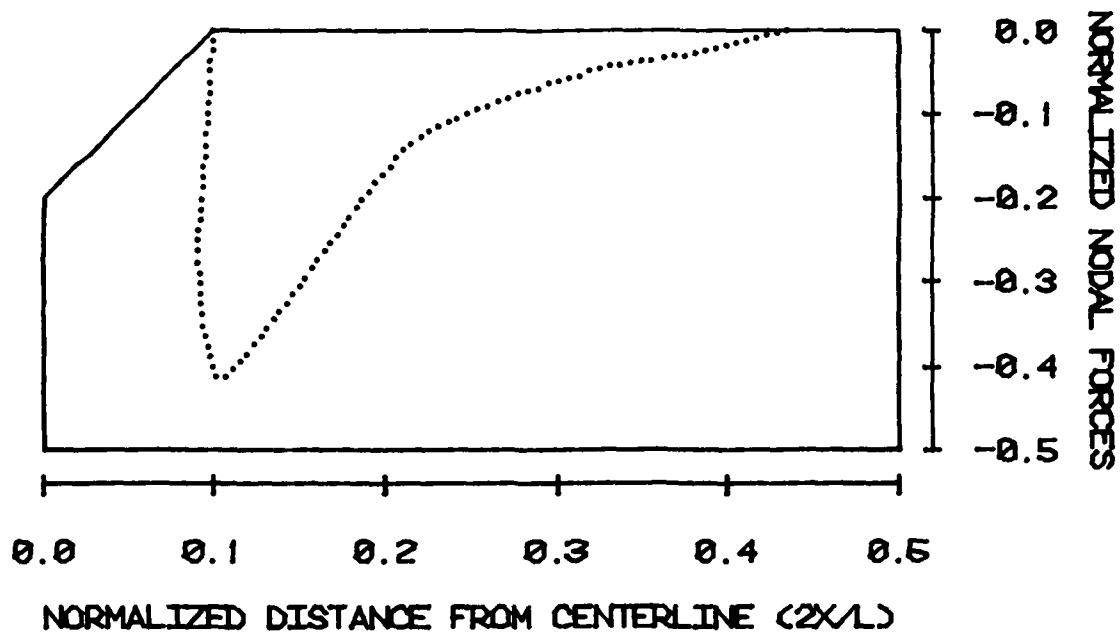


Figure 13. Normalized Nodal Reaction Forces F_n/P_{Total} at the Upper Center Loading Surface.

CENTERLINE SHEAR STRESS DISTRIBUTION

$$E_{11}/E_{22} = 1.0$$

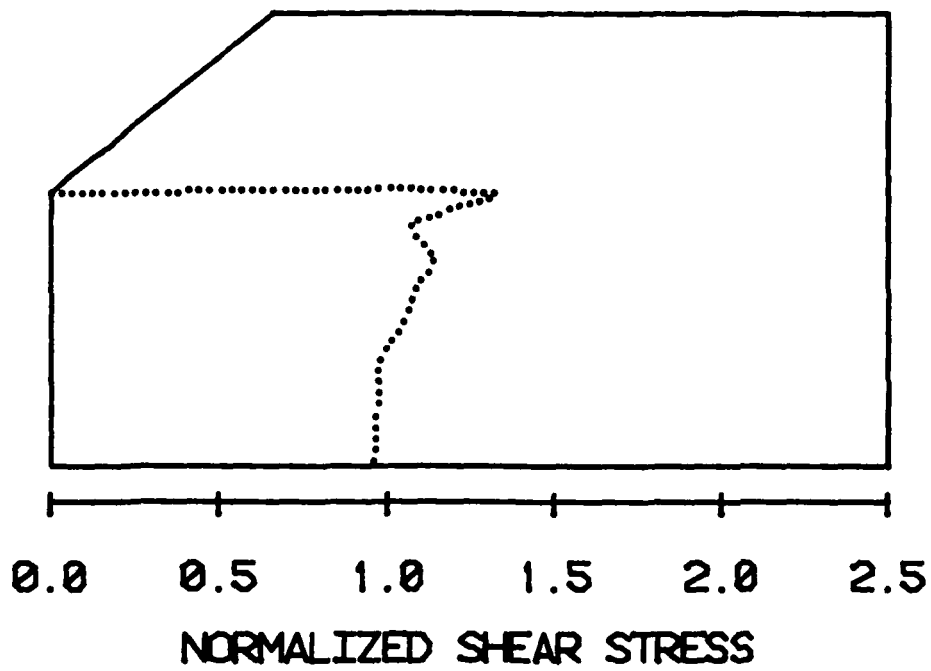


Figure 14. Normalized Shear Stress Distribution τ_{xy}/τ at the Specimen Vertical Centerline for an Orthotropy Ratio of 1.0.

Another region of interest in the specimen is that covered by the strain gages used for strain and modulus determinations. This strain measuring region can be visualized in the strain-gaged specimen photograph previously shown as Figure 6. This region is outlined by the heavier solid lines in the expanded finite element grid plot shown in Figure 15. The normalized stress contours for this region are plotted in Figures 16 through 18. The bending stresses (and hence also the strains) are very low in this region relative to the average applied shear stress. Contour values are no higher than 0.05, as shown in Figure 16. Compressive σ_y stresses do appear to be a problem, however, as indicated in Figure 17. Normalized stress contour values $\sigma_y/|\bar{\tau}|$ are as high as -0.64, indicating a strong loading point influence within the region. Shear stresses beneath the strain gages are uniform, but low. This would result in an artificially high shear modulus calculation. The calculated shear modulus based on the average shear strain measured within the strain gage region and the average applied shear stress is 30 GPa (4.37 Msi). This is 9.8 percent greater than the input shear modulus of 28 GPa (3.98 Msi).

3.3.2 Orthotropic Material ($E_{11}/E_{22} = 13.3$)

The primary interest in this test method is for use with orthotropic composite materials rather than isotropic metals. Therefore, two different unidirectional composite materials were also modeled. The fiber direction was assumed to be parallel to the x-axis (longitudinal axis) of the test specimen. Normalized stress contour plots for the $E_{11}/E_{22} = 13.3$ orthotropy ratio material (AS/3501-6 graphite/epoxy) are presented as Figures 19 through 21. These three plots all show expanded views of the region containing the upper notch.

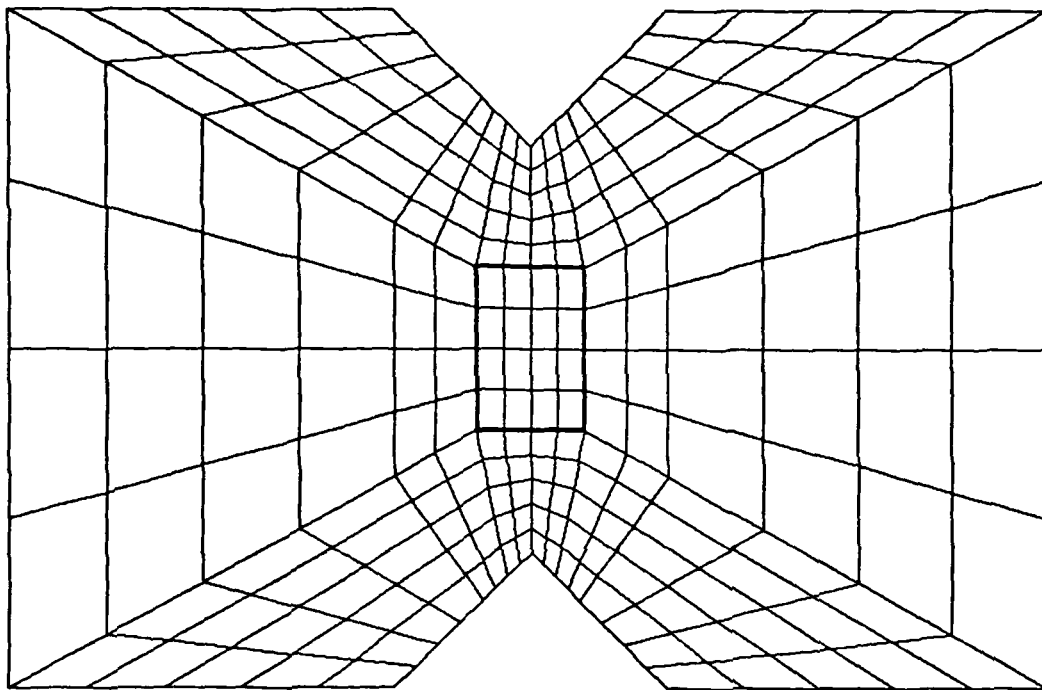


Figure 15. Expanded Finite Element Grid Plot Indicating the Region in Which Strain Gages Would Normally be Attached to the Iosipescu Specimen.

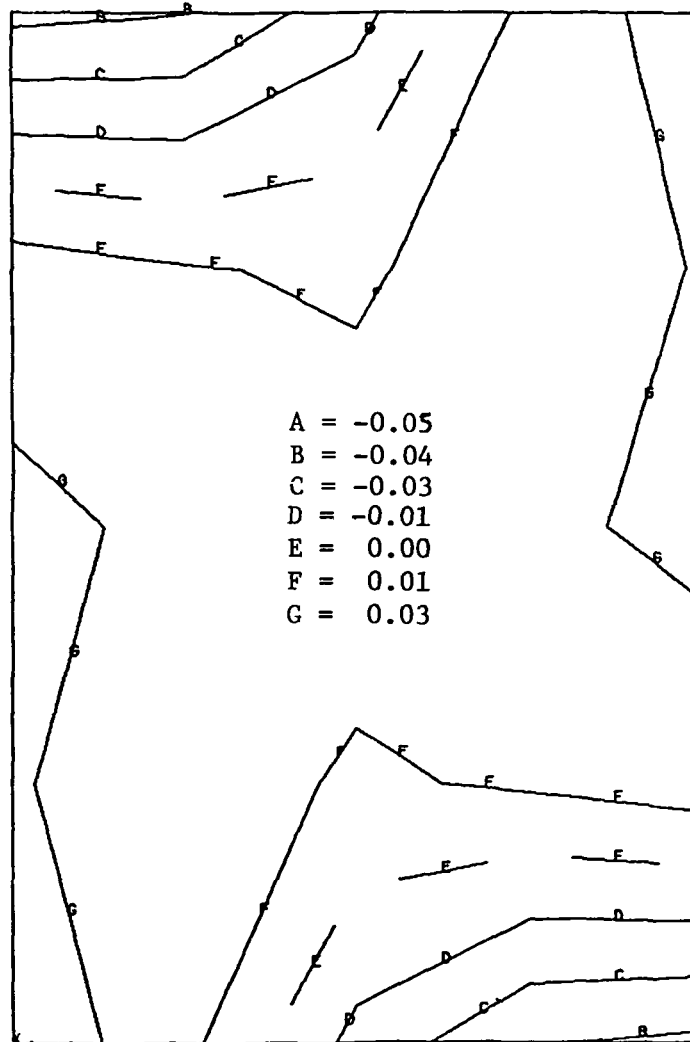


Figure 16. Normalized Bending Stress Contours $\sigma_x/|\bar{\tau}|$ in the Strain Gaged Region (see Figure 15) for an Orthotropy Ratio of 1.0.

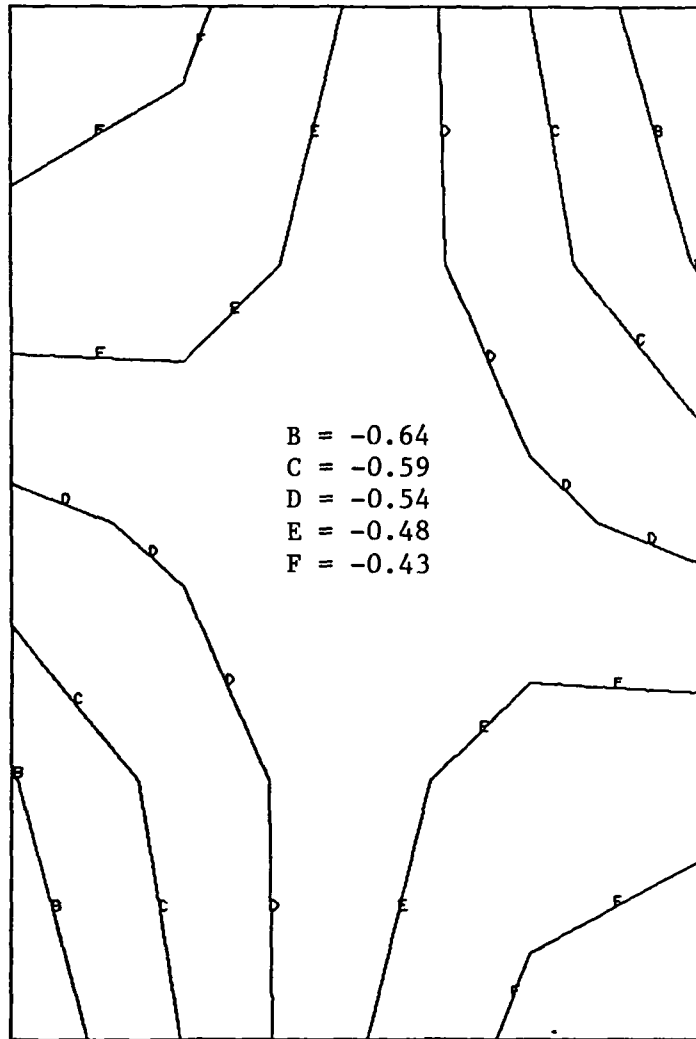


Figure 17. Normalized Transverse Normal Stress Contours $\sigma_y/|\bar{\tau}|$ in the Strain Gaged Region (see Figure 15) for an Orthotropy Ratio of 1.0.

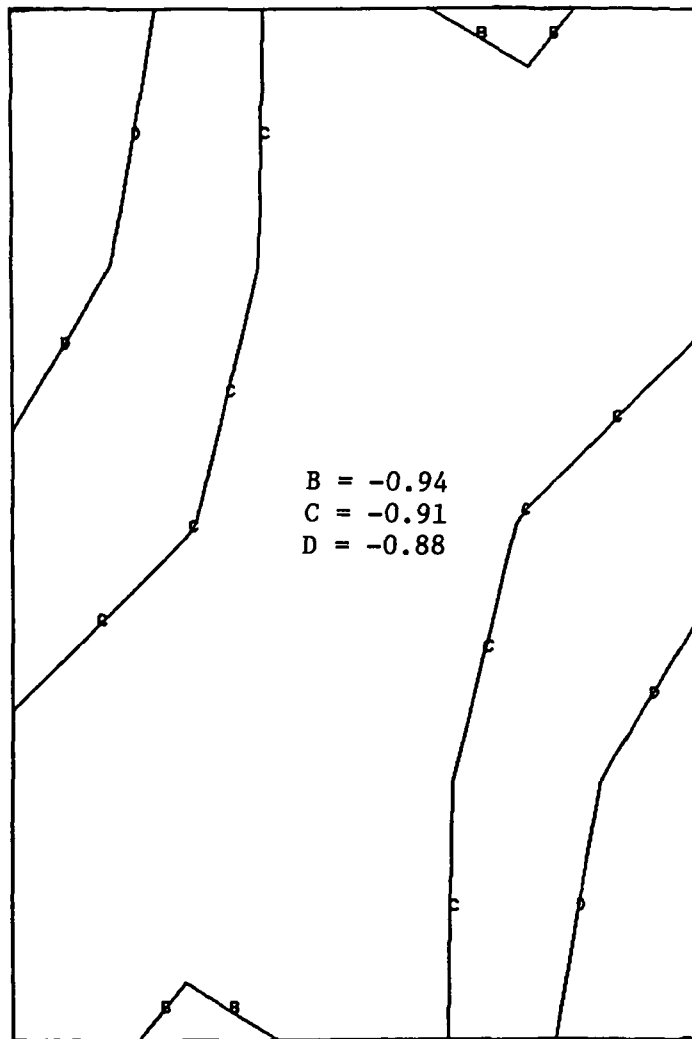


Figure 18. Normalized Shear Stress Contours $\tau_{xy}/|\tau|$ in the Strain Gaged Region for an Orthotropy Ratio of 1.0.

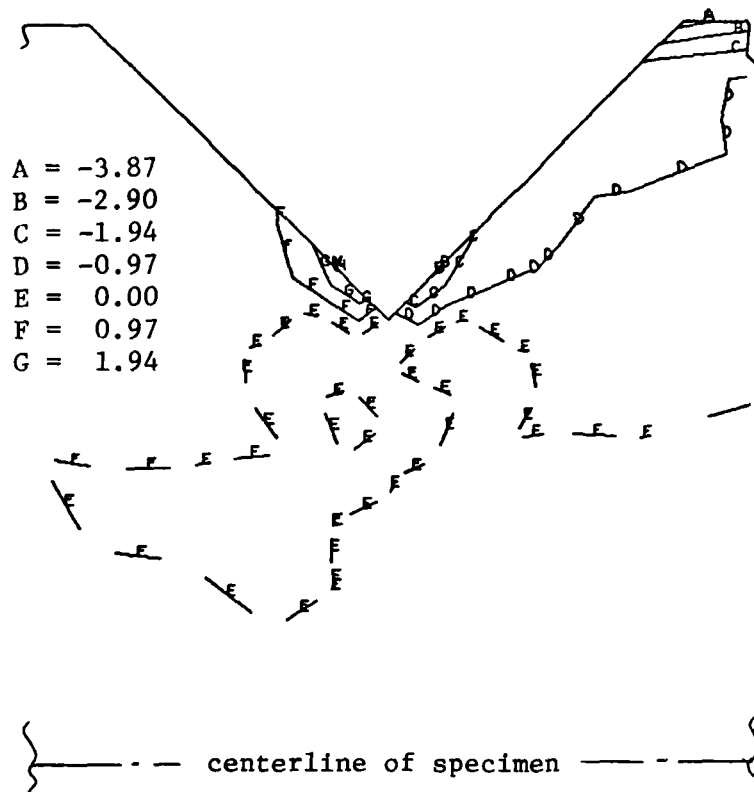


Figure 19. Normalized Bending Stress Contours $\sigma_x/|\bar{\tau}|$ in the Notch Region for an Orthotropy Ratio of 13.3

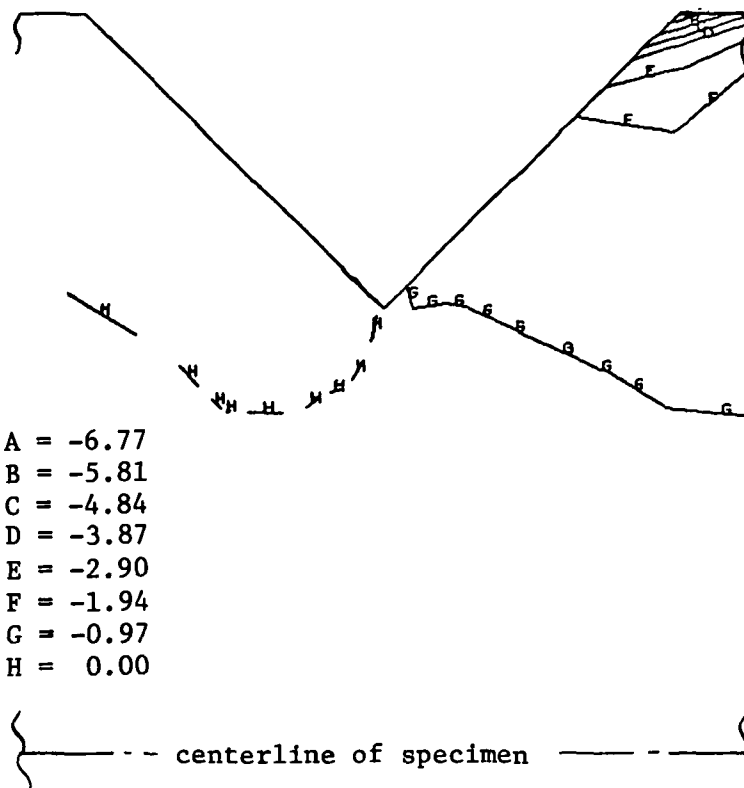


Figure 20. Normalized Transverse Normal Stress Contours $\sigma_y / |\bar{\tau}|$ in the Notch Region for an Orthotropy Ratio of 13.3.

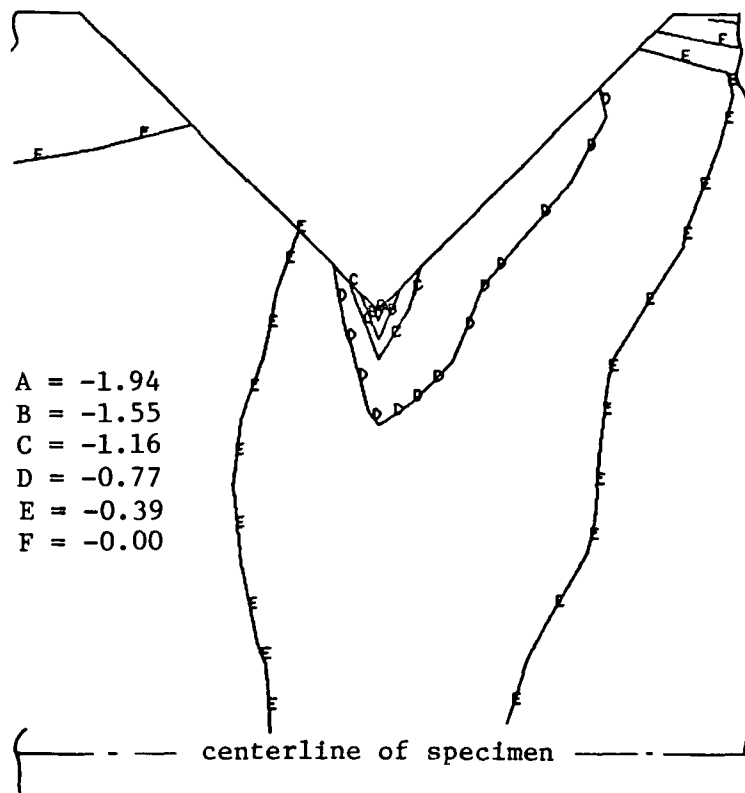


Figure 21. Normalized Shear Stress Contours $\tau_{xy}/|\bar{\tau}|$ in the Notch Region for an Orthotropy Ratio of 13.3.

Looking first at Figure 19, it can be seen that the major portion of the test section is free of σ_x (bending-induced) stresses. However, significant bending stresses are present at short distances on either side of the notch root, as would be expected. Comparing Figure 19 to Figure 10 it can be seen that the shapes of the contours are very similar. In particular, the D and F contours of Figure 19 are quite similar in shape to the F and H contours in Figure 10. However, the magnitudes of the contours in Figure 19 are almost twice as great at the corresponding stress contours in Figure 10. The reason for this behavior can be explained by examining the E_{11}/G_{12} ratios for each material. The isotropic aluminum has a modulus ratio of $E_{11}/G_{12} = 2(1 + \nu) = 2.66$. The orthotropic ($E_{11}/E_{22} = 13.3$) AS/3501-6 unidirectional graphite/ epoxy has a longitudinal modulus to shear modulus ratio of $E_{11}/G_{12} = 25$, based on the input material properties listed in Table 2. This means that for a given shear displacement introduced by the Iosipescu shear fixture, the normalized bending stresses $\sigma_x/|\bar{\tau}|$ will be greater for the orthotropic material. This is due to a higher longitudinal modulus resulting in higher bending stresses and lower applied shear stress due to a much lower shear modulus.

Normalized transverse normal stress contours $\sigma_y/|\bar{\tau}|$ are plotted in Figure 20. As was the case in Figure 11, very high compressive stresses are introduced near the loading point to the right of the notch. These large stresses do intrude into the test section. The normalized stress contours G and H of Figure 20 are similar in appearance and magnitude to the E and F contours of Figure 11. The effect of the loading points appears to be similar for both materials.

The normalized shear stress contours for the $E_{11}/E_{22} = 13.3$ orthotropy ratio material plotted in Figure 21 exhibit the same shear stress concentration effect as was noted for the isotropic material normalized shear stress contours plotted in Figure 12. The effect of this shear stress concentration at the root of the notch is greater for the orthotropic material, the normalized shear stress reaching a magnitude of -2.01 near the root of the notch. Some caution must be observed when discussing actual numerical stress values in this region, due to the coarseness of the mesh at this point. However, the trends are at least qualitatively demonstrated, if not quantitatively. Also, results published by Herakovich and Bergner [38] showed a value of normalized shear stress of -1.95 at the notch root for a 17.7 orthotropy ratio material.

This shear stress concentration is further emphasized by the shear stress distribution plot shown as Figure 22. These results help explain the shear failures obtained previously by the present authors for unidirectional graphite/epoxy [24]. A typical failed specimen is shown in Figure 23. Despite the surface appearance (caused by the imprint of the bleeder ply during fabrication), the specimen is actually unidirectional graphite/epoxy, with the fibers parallel to the horizontal direction. This specimen has cracks originating between the notch roots, propagating outward parallel to the fiber direction. These cracks are probably due to shear failures, based on the fact that the predicted shear stresses are high in the notch tip region and the material shear strength is low relative to its longitudinal tensile strength. The cracks are probably not caused by transverse tensile stresses as the transverse stresses are predicted to be low, or negative

CENTERLINE SHEAR STRESS DISTRIBUTION

$$E_{11}/E_{22} = 13.3$$

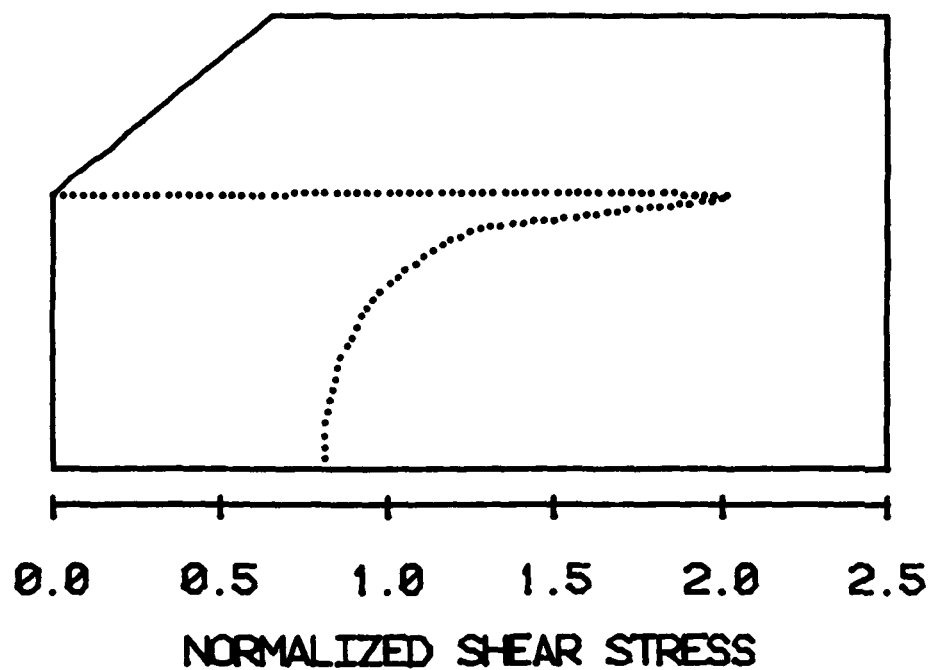


Figure 22. Normalized Shear Stress Distribution τ_{xy}/τ at the Vertical Centerline for an Orthotropy Ratio of 13.3.

ORIGINAL PAGE IS
OF POOR QUALITY

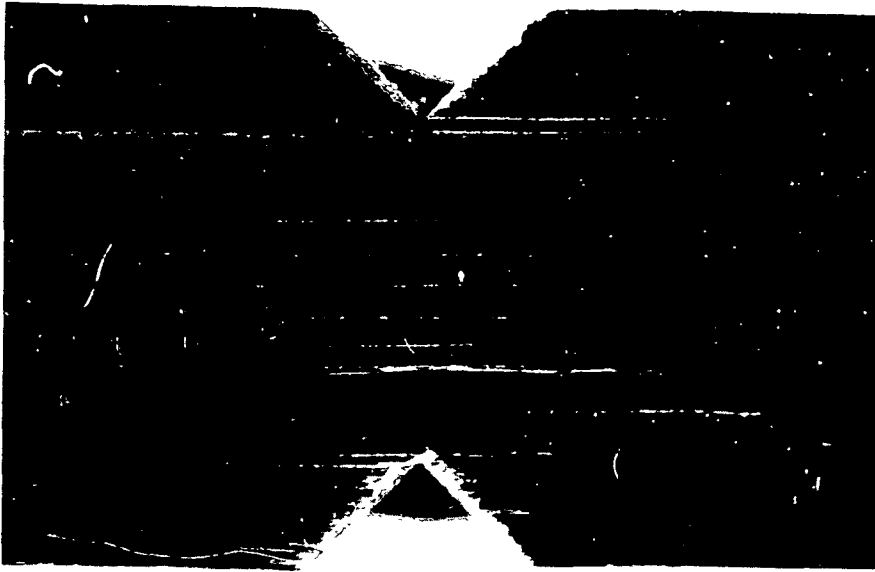


Figure 23. Failed Iosipescu Shear Specimen of Unidirectional Graphite/Epoxy Composite.

(compressive), near the notch region (see Figure 20). Although not evident in this failed specimen, the first cracks occurred at the notch roots, as the shear stress concentration indicated in Figure 22 would suggest.

Figures 24 through 26 show normalized stress contours plotted in the region of the strain gages. Again, there is little bending stress predicted beneath the strain gages, as shown in Figure 24. Significant transverse compressive stresses are present, shown in Figure 25, due to the proximity of the loading points. Finally, the shear stress distribution shown in Figure 26 is relatively uniform, although low (i.e., the normalized values are less than one). The measured shear modulus would therefore be calculated to be about 22 percent too high for the 13.3 orthotropy ratio material.

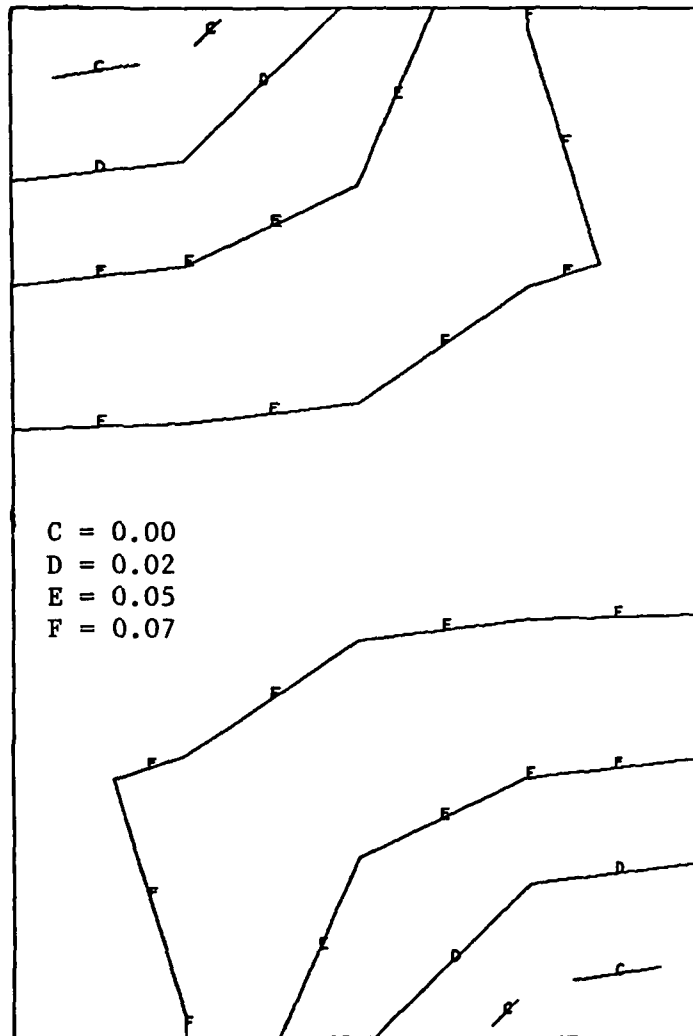


Figure 24. Normalized Bending Stress Contours $\sigma_x / |\bar{\tau}|$ in the Strain Gaged Region for an Orthotropy Ratio of 13.3.

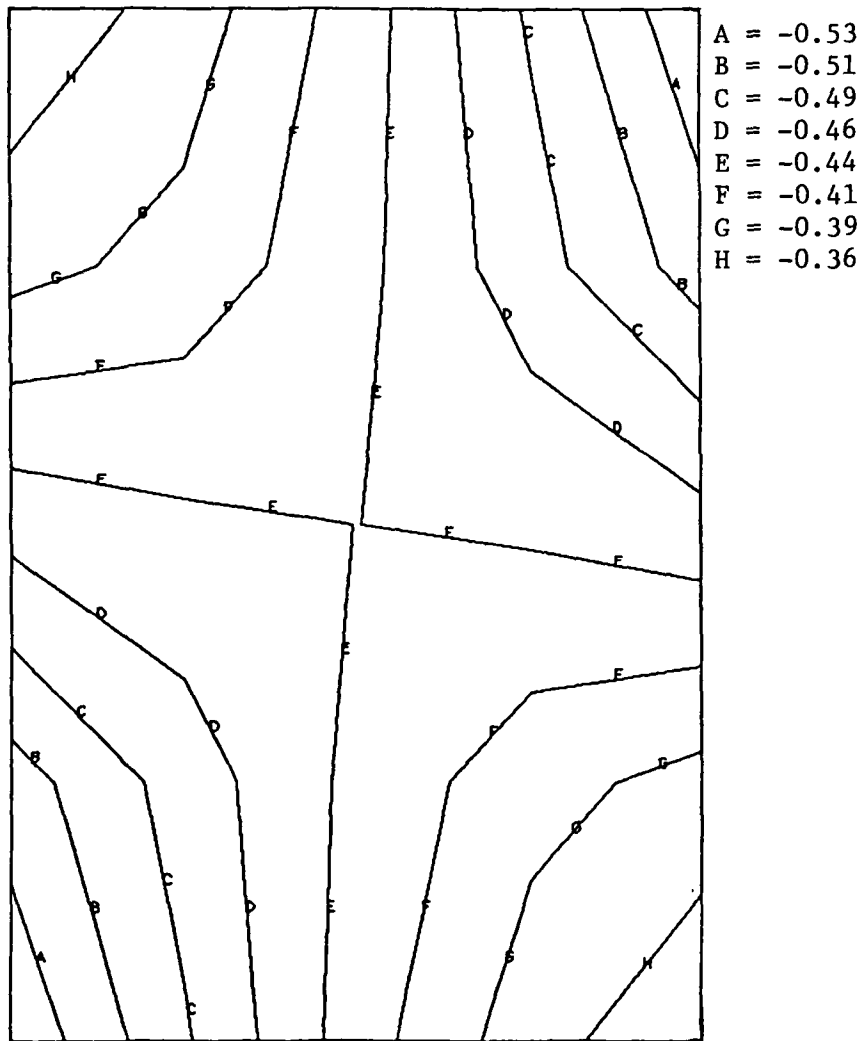


Figure 25. Normalized Transverse Normal Stress Contours $\sigma_y/|\bar{\tau}|$ in the Strain Gaged Region for an Orthotropy Ratio of 13.3.

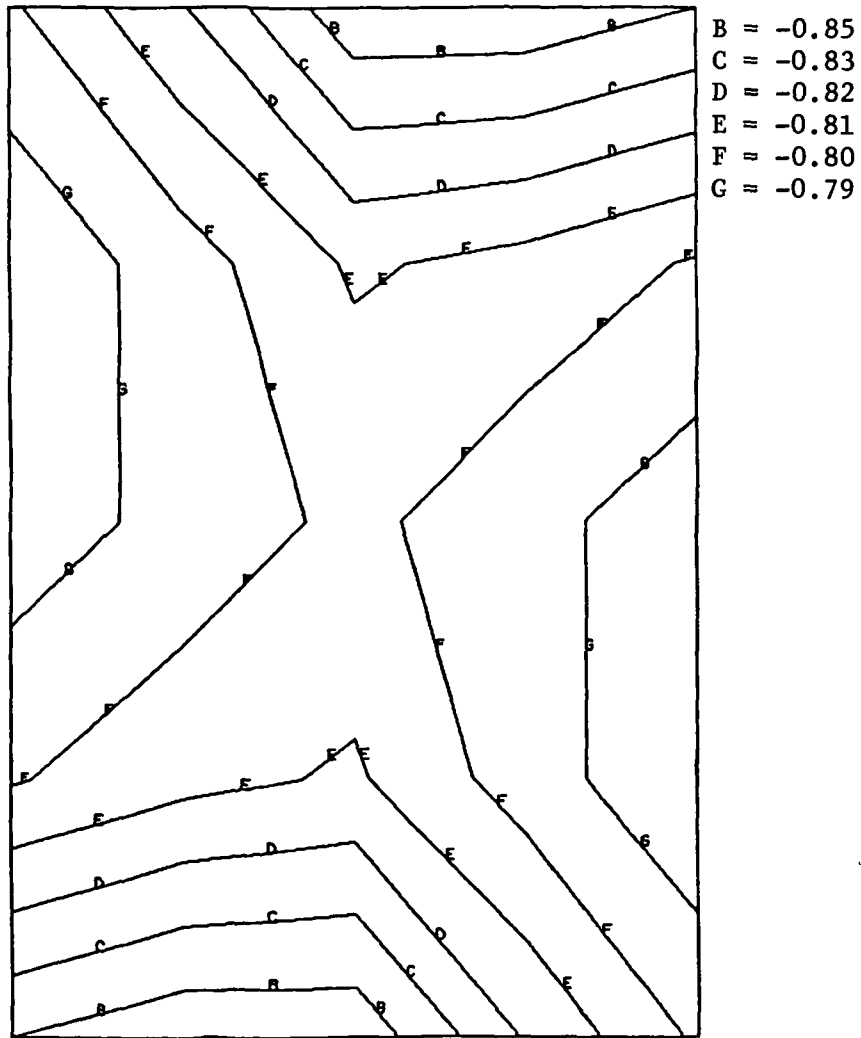


Figure 26. Normalized Shear Stress Contours $\tau_{xy}/|\bar{\tau}|$ in the Strain Gaged Region for an Orthotropy Ratio of 13.3.

3.3.3 Highly Orthotropic Material ($E_{11}/E_{22} = 49.4$)

Results for the higher orthotropy ratio composite material ($E_{11}/E_{22} = 49.4$) follow the same trends indicated previously for the 1.0 and 13.3 orthotropy ratio materials. In the 49.4 orthotropy ratio material test specimen, the bending stresses are quite high around the root of the notch, as shown in Figure 27. The bending stresses are greater in the 49.4 orthotropy ratio material (Figure 27) than in the 13.3 orthotropy ratio material (Figure 19), which in turn were greater than for the isotropic material (Figure 10). Normalized transverse normal stress contours for the 49.4 orthotropy ratio material are plotted in Figure 28. Again the stresses are low within the test region, but compressive stresses from the loading surfaces do intrude into the test region. Normalized shear stresses for the 49.4 orthotropy ratio material are plotted in Figure 29. Again there is a predicted shear stress concentration effect due to the presence of the notch. The maximum normalized shear stress is 2.42 for this case. Comparing Figure 29 to Figures 21 and 12, it can be seen that the shear stress concentration effect increases with increasing orthotropy ratio. This can be further illustrated by comparing the centerline shear stress distribution profile shown in Figure 30 for the 49.4 orthotropy ratio material with the shear stress distribution plots for the 13.4 and 1.0 orthotropy ratio materials, Figures 22 and 14, respectively.

Stress contour plots within the strain gage region for the 49.4 orthotropy ratio material were very similar to those plots already presented; therefore they won't be included here. Basically, beneath the strain gages, the bending stresses were small. Significant transverse normal compressive stresses introduced at the loading

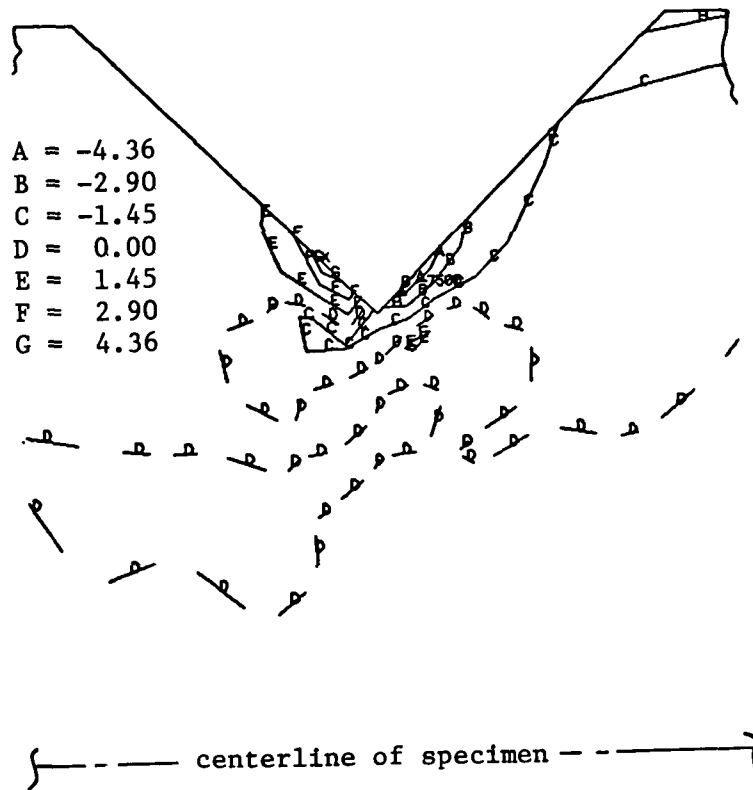
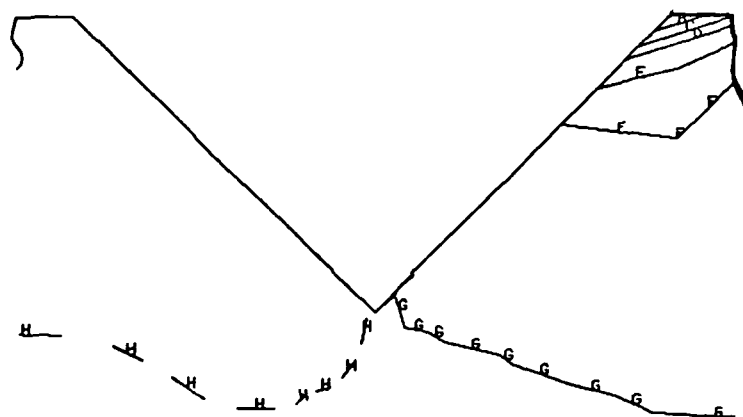


Figure 27. Normalized Bending Stress Contours $\sigma_x/|\bar{\tau}|$
 in the Notch Region for an Orthotropy
 Ratio of 49.4.



A =	-6.35
B =	-5.45
C =	-4.54
D =	-3.63
E =	-2.72
F =	-1.82
G =	-0.91
H =	0.00

} ----- centerline of specimen ----- }

Figure 28. Normalized Transverse Normal Stress Contours $\sigma_y / |\tau|$ in the Notch Region for an Orthotropy Ratio of 49.4.

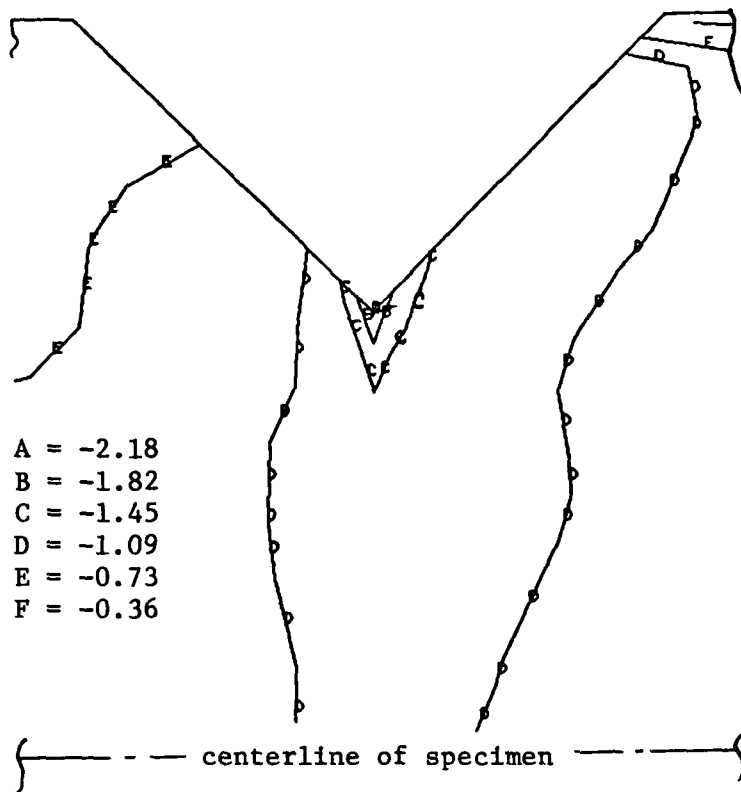


Figure 29. Normalized Shear Stress Contours $\tau_{xy}/|\bar{\tau}|$
 Notch Region for an Orthotropy
 Ratio of 49.4.

CENTERLINE SHEAR STRESS DISTRIBUTION

$$E_{11}/E_{22} = 49.4$$

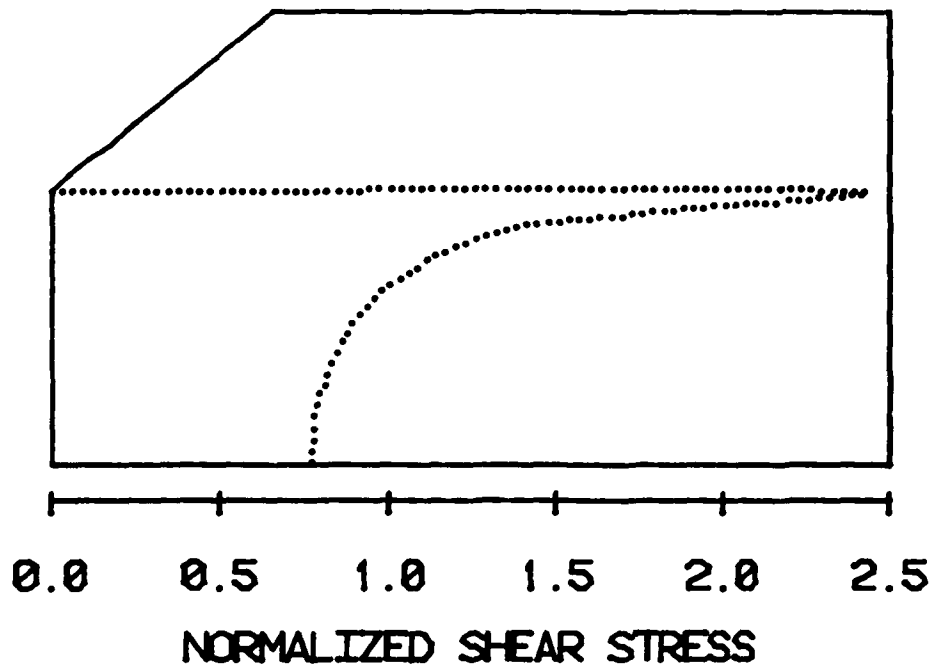


Figure 30. Normalized Shear Stress Distribution $\tau_{xy}/\bar{\tau}$ at the Vertical Centerline for an Orthotropy Ratio of 49.4.

surfaces were present. The shear stress contours were reasonably uniform, but again low. The error in measured shear modulus for this case would have been 29 percent.

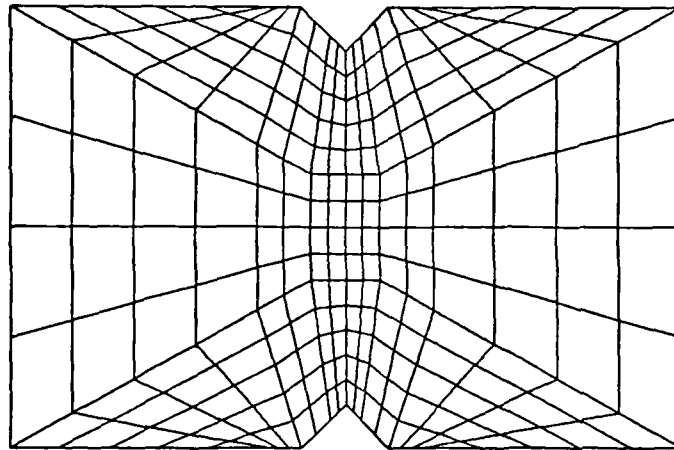
3.3.4 Summary

To summarize the analytical results obtained here for the current Wyoming version of the Iosipescu Shear Test, the test does appear to produce a relatively pure state of shear within the test specimen. There does appear to be some shear stress concentration due to the presence of the notch, but normal stresses are relatively unaffected. Bending stresses may be large in highly orthotropic materials. The loading points nearest the notches are too close to the test section of the specimen and should be moved. This will be pursued both analytically and experimentally in the second-year follow-on effort. In the following paragraphs possible notch geometry variations will be discussed, in an effort to establish the optimum test specimen configuration for materials of differing orthotropy ratios.

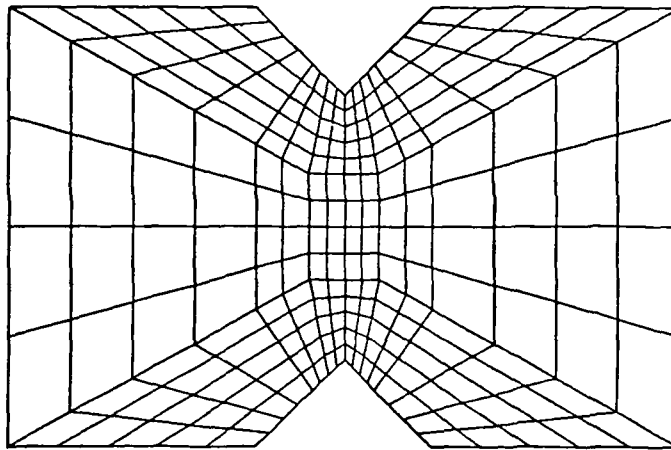
3.4 Effect of Notch Depth

Iosipescu originally concluded that the optimum notch depth was 22.5 percent of the width, but he used notch depths of 25 percent in his experimental work [21]. The present Wyoming version of the Iosipescu Shear Test uses notch depths of 20 percent. Analytically, notch depths of 10, 20, and 30 percent were modeled. Finite element mesh plots for the notch regions are shown in Figure 31 for the three depths modeled. The tip radius was modeled as being very sharp, i.e., for a tip radius equal to zero.

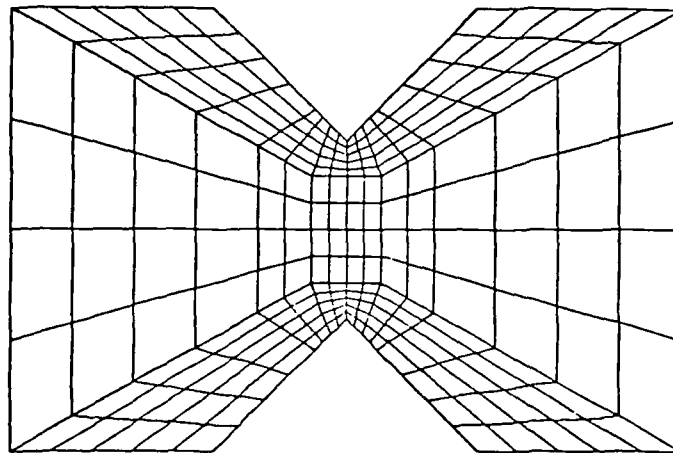
The analysis was performed for all three orthotropy ratio materials. Normalized centerline shear stress distributions are plotted



a) notch depth = 10 percent



b) notch depth = 20 percent



c) notch depth = 30 percent

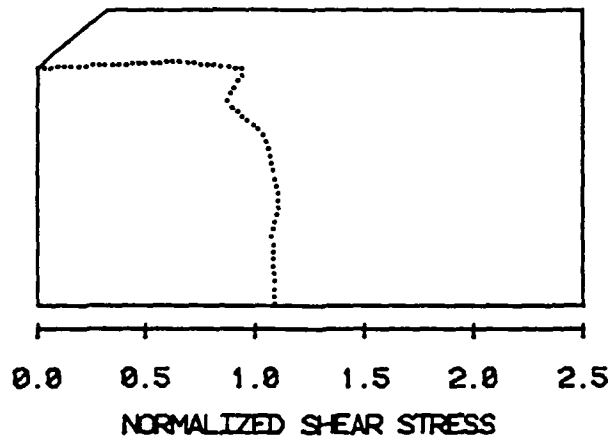
Figure 31. Finite Element Grids Used to Model Different Notch Depths; Notch Angle = 90° and Notch Tip Radius = 0.00 mm.

in Figures 32 through 34 for the 1.0, 13.3 and 49.4 orthotropy ratio materials, respectively. Basically, all three materials react in a similar manner to the different notch depths. Looking first at Figure 32a, it can be seen that the shear stress is less at the notch root, tending to increase towards the center of the specimen. This stress profile, for a shallow notch, is tending towards the parabolic distribution which would be observed in a straight beam, i.e., a specimen with a notch depth of zero. The shear stress distribution shown in Figure 32b tends to be relatively constant around a value of one. The optimum profile, of course, is a straight line at one. One should not place too much importance on each small change in the curve; these irregularities may be due to the coarseness of the finite element mesh used. There does seem to be a shear stress concentration effect at the notch root, however, as the profile tends to rise as the notch is approached in Figure 32. This stress rise is more likely an effect of tip radius rather than notch depth.

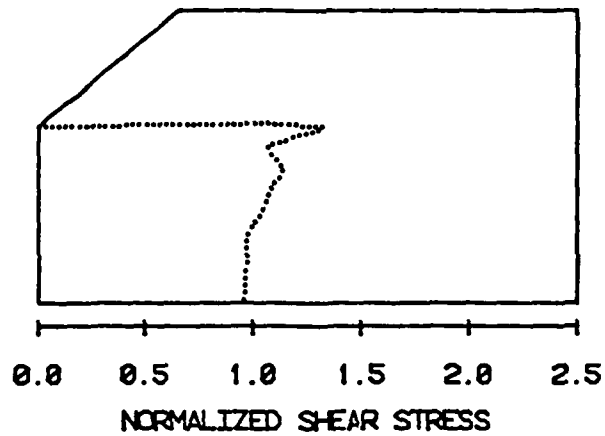
Shear stress distributions in the orthotropic materials, Figures 33 and 34, are not as uniform as the stress distributions in the isotropic material, Figure 32. However, the same trends with varying notch depth may be observed. Peak shear stresses are slightly higher for the 20 percent notch depth than for the 10 percent notch depth, then slightly lower again for the 30 percent notch depth. It is not understood at this time why the peak stress goes down for the 30 percent notch depth relative to the 20 percent notch depth. The change is not drastic, and there are almost no changes in the shapes of the shear stress distributions in going from 20 percent to 30 percent notch depths.

Overall, the notch depth does have some influence on the shear

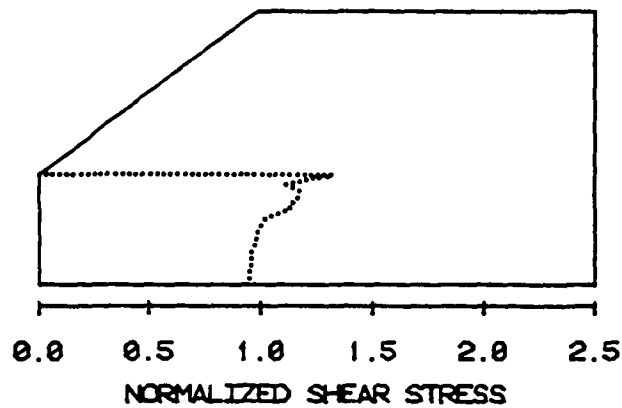
CENTERLINE SHEAR STRESS DISTRIBUTION
 $E_{11}/E_{22} = 1.0$



a) notch depth = 10 percent



b) notch depth = 20 percent

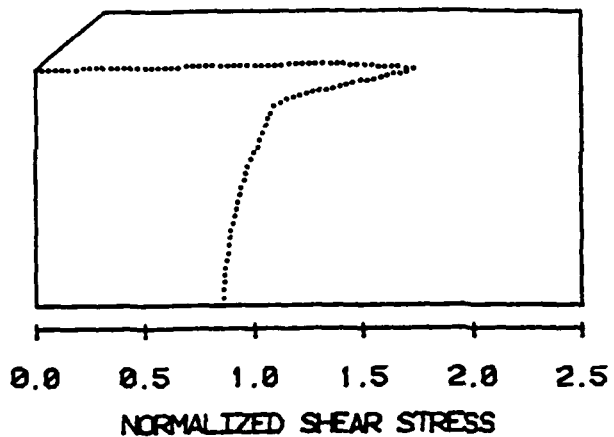


c) notch depth = 30 percent

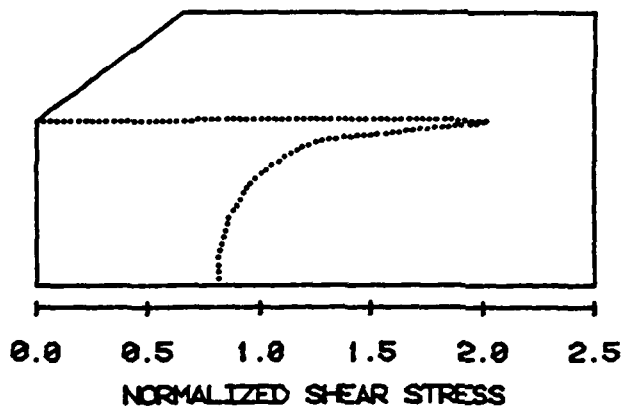
Figure 32. Effect of Notch Depth on the Normalized Shear Stress Distribution $\tau_{xy}/\bar{\tau}$ Distribution Across the Notches for an Orthotropy Ratio of 1.0; Notch Angle = 90° , Notch Tip Radius = 0.00 mm.

CENTERLINE SHEAR STRESS DISTRIBUTION

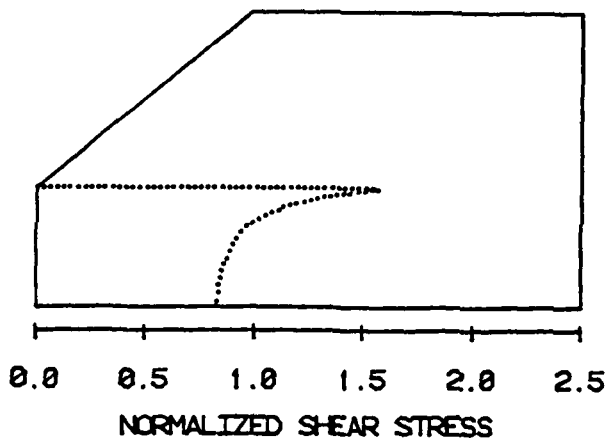
$E_{11}/E_{22} = 13.3$



a) notch depth = 10 percent



b) notch depth = 20 percent

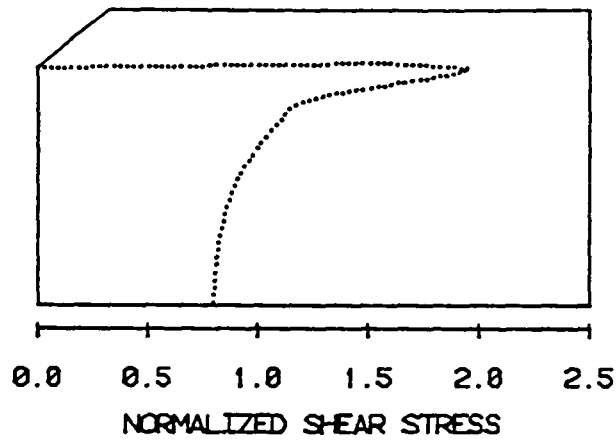


c) notch depth = 30 percent

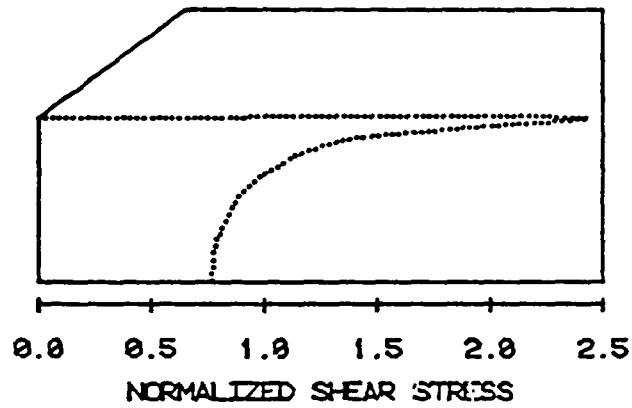
Figure 33. Effect of Notch Depth on the Normalized Shear Stress Distribution $\tau_{xy}/\bar{\tau}$ for an Orthotropy Ratio of 13.3; Notch Angle = 90° , Notch Tip Radius = 0.00 mm.

CENTERLINE SHEAR STRESS DISTRIBUTION

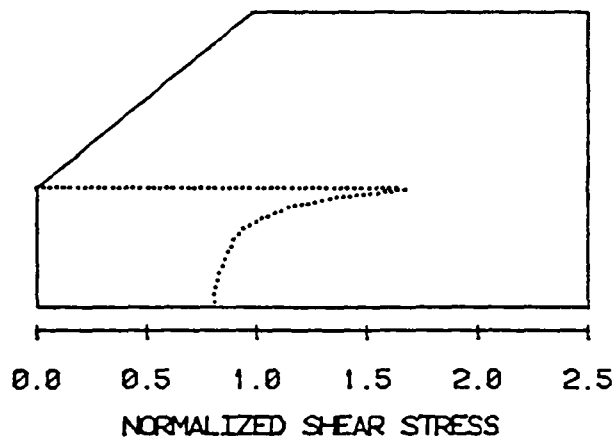
$E_{11}/E_{22} = 49.4$



a) notch depth = 10 percent



b) notch depth = 20 percent



c) notch depth = 30 percent

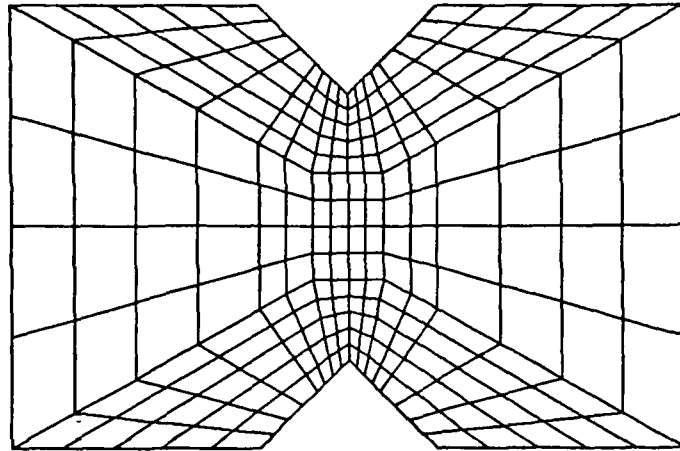
Figure 34. Effect of Notch Depth on the Normalized Shear Stress Distribution $\tau_{xy}/\bar{\tau}$ for an Orthotropy Ratio of 49.4, Notch Angle = 90° , Notch Tip Radius = 0.00 mm.

stress distribution. However, over the practical range of notch depths modeled in this program, notch depth appears to have minimal influence relative to other notch geometry factors.

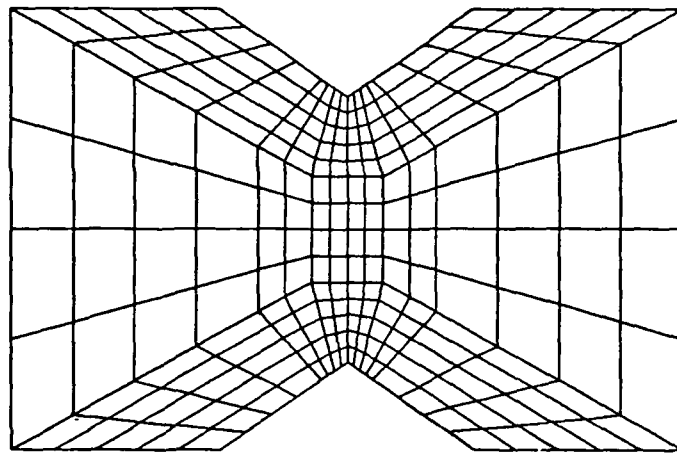
3.5 Effect of Notch Angle

Iosipescu's original argument for using a 90° included angle notch was that because the sides of the notch were aligned with the principal normal stress planes, the principal normal stresses would be zero at the notch. Therefore the notch would not act as a stress concentrator, its only function being to force the shear stress distribution to a uniform value as opposed to the parabolic distribution in a straight sided beam. Strictly from a classical stress transformation viewpoint, there is no reason to change the notch angle just because the material is orthotropic rather than isotropic. The principal stresses remain the same. However, the principal stresses are not usually of great interest when studying orthotropic composite materials. The purpose of the present study was to determine if there is a more favorable notch angle, perhaps one depending on the orthotropy ratio of the material. As was listed in Table 2, three notch angles were analyzed, viz, the current 90° configuration, as well as 110° and 120° . Finite element mesh plots in the notch regions of the models are shown in Figure 35. The current standard 20 percent notch depth and 0.00 mm notch tip radius were modeled for each of the three different angles.

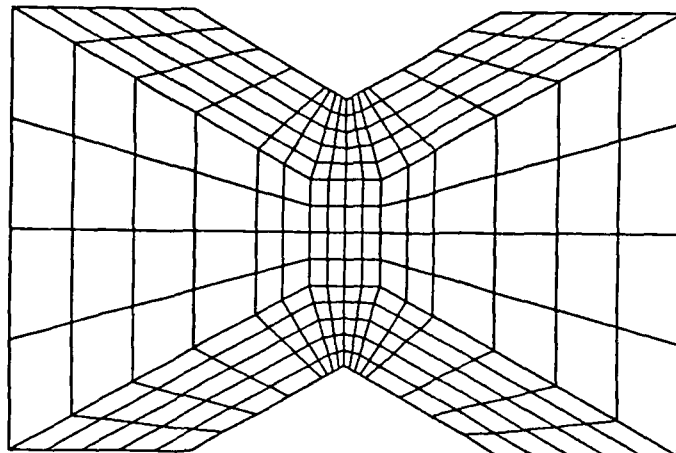
Normalized shear stress distributions for the isotropic aluminum material are plotted in Figure 36. The effect of increasing notch angle (Figure 36c) appears to be similar to the effect of a reduced notch depth, (Figure 32a). Basically, the shear stress tends to be lower at the notch, increasing towards the specimen center. A notch angle of



a) notch angle = 90°



b) notch angle = 110°

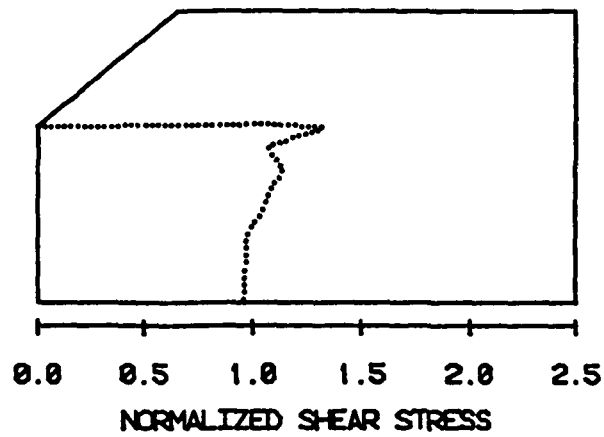


c) notch angle = 120°

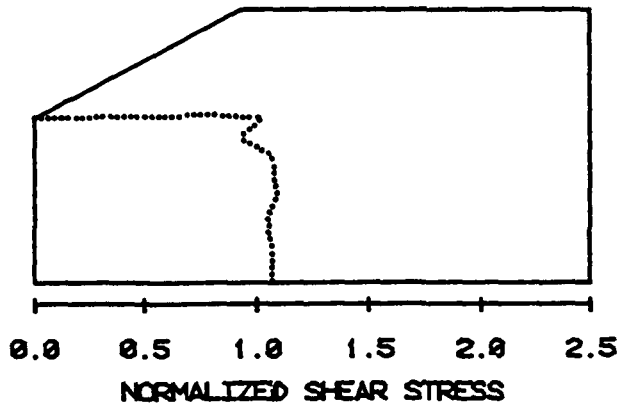
Figure 35. Finite Element Grids Used to Model Different Notch Angles; Notch Depth = 20 Percent, Notch Tip Radius = 0.00 mm.

CENTERLINE SHEAR STRESS DISTRIBUTION

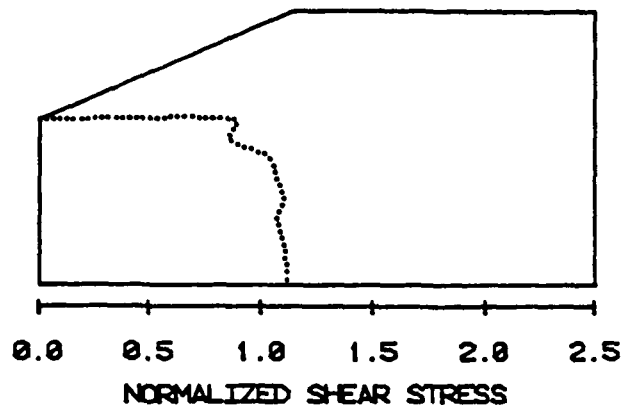
$E_{11}/E_{22} = 1.0$



a) notch angle = 90°



b) notch angle = 110°



c) notch angle = 120°

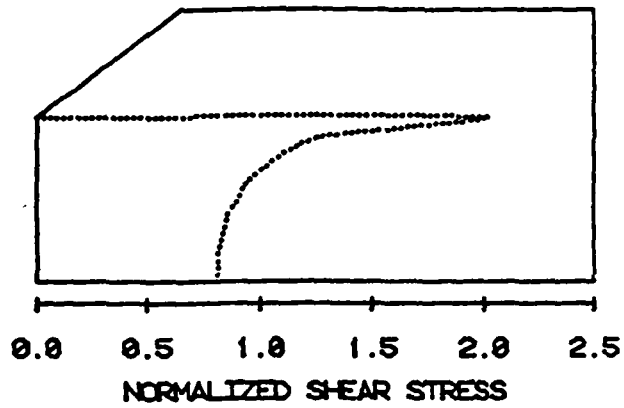
Figure 36. Effect of Notch Angle on the Normalized Shear Stress Distribution $\tau_{xy}/\bar{\tau}$ Across the Notches for an Orthotropy Ratio of 1.0; Notch Depth = 20 Percent, Notch Tip Radius = 0.00 mm.

110°, Figure 36b, appears to produce the most uniform shear stress distribution. There is still some shear stress concentration at the notch tip. Again, however, the finite element mesh is fairly coarse, and the slight stress distribution anomalies indicated may or may not actually exist at the notch tip. Surprisingly, there are very few changes in bending stress σ_x or transverse normal stress σ_y contours with changing notch angle. These plots for the 110° and 120° notch angles are essentially the same as those shown in Figures 10 for the 90° notch angle.

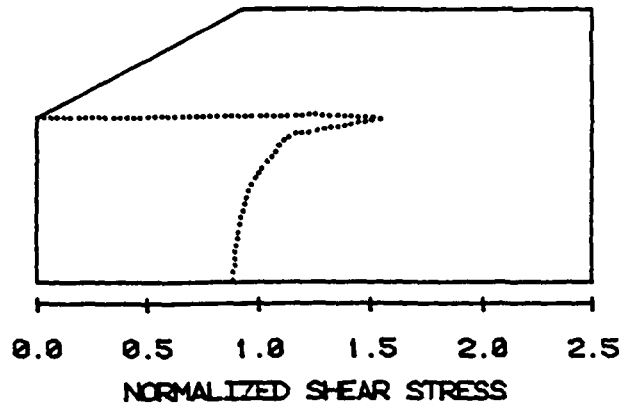
Centerline shear stress distributions as a function of notch angle for the orthotropic materials are shown in Figures 37 and 38. The same general trends are evident for the orthotropic materials as were observed for the isotropic material. Essentially, the higher notch angles tend to reduce the shear stress concentration of the notch. However, the shear distributions shown in Figures 37 and 38 are still far from the desirable uniform distribution.

Normalized bending stress and transverse normal stress contours are essentially unchanged with increasing notch angle for the orthotropic materials as well. These contour plots are approximately the same as the corresponding contour plots for a 90° notch angle, shown in Figures 19 through 20 and 27 through 28. Normalized shear stress contour plots are affected by increasing notch angle for all three materials, as can be seen in Figures 39 through 41. The higher notch angles tend to slightly broaden the relatively constant shear stress region at the center of the test specimen. The contour shapes also tend to rotate with larger notch angle. Note the steep shear stress gradients in Figures 40a and 41a, which are reduced by the wider notch angles, as

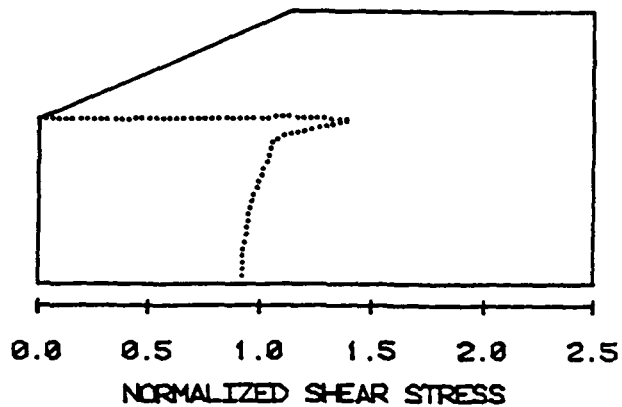
CENTERLINE SHEAR STRESS DISTRIBUTION
 $E_{11}/E_{22} = 13.3$



a) notch angle = 90°



b) notch angle = 110°

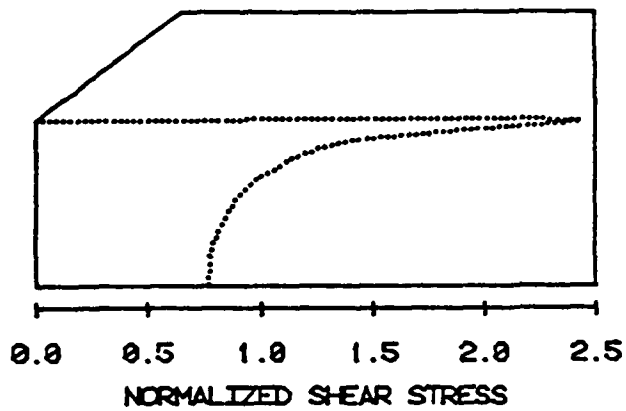


c) notch angle = 120°

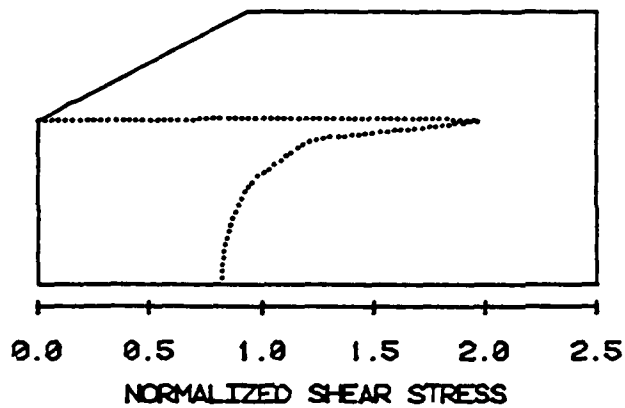
Figure 37. Effect of Notch Angle on the Normalized Shear Stress Distribution $\tau_{xy}/\bar{\tau}$ Across the Notches for an Orthotropy Ratio of 13.3; Notch Depth = 20 Percent, Notch Tip Radius = 0.00 mm.

CENTERLINE SHEAR STRESS DISTRIBUTION

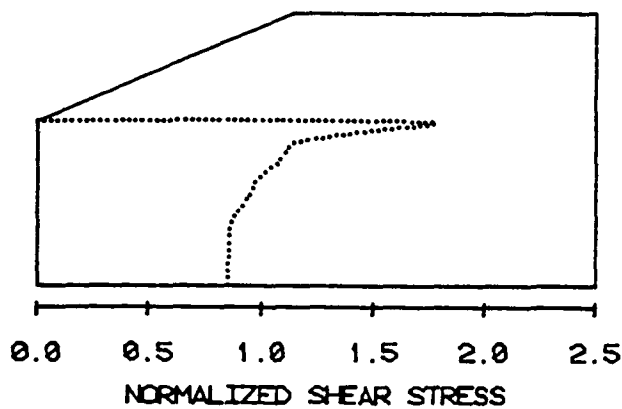
$E_{11}/E_{22} = 49.4$



a) notch angle = 90°

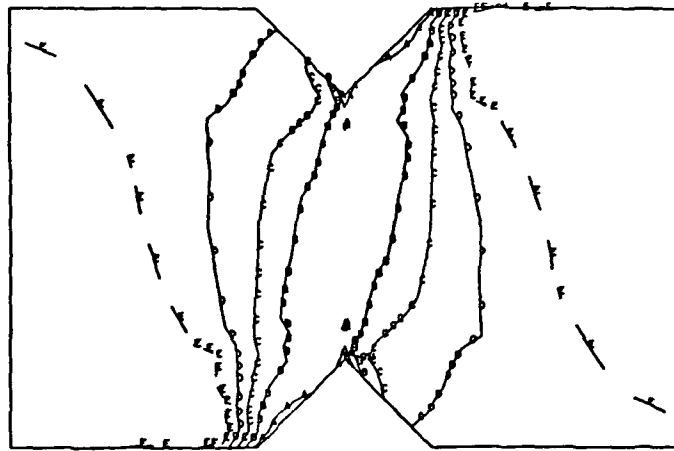


b) notch angle = 110°



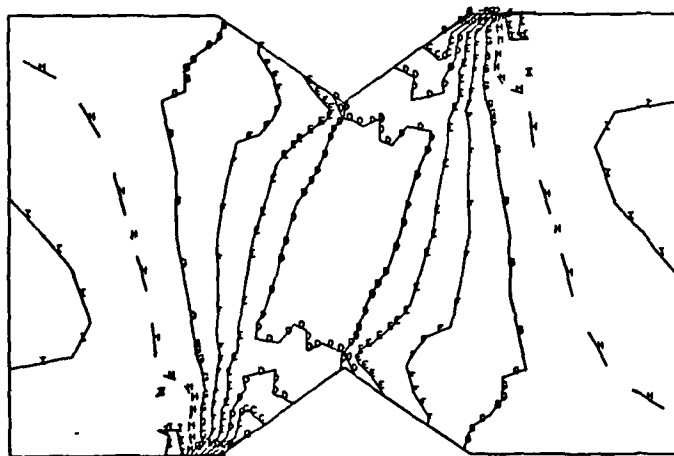
c) notch angle = 120°

Figure 38. Effect of Notch Angle on the Normalized Shear Stress Distribution $\tau_{xy}/\bar{\tau}$ Across the Notches for an Orthotropy Ratio of 49.4; Notch Depth = 20 Percent, Notch Tip Radius = 0.00 mm.



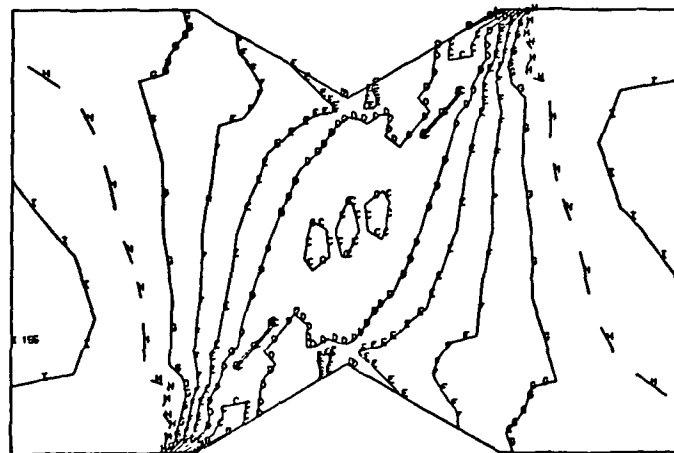
A = -1.07
 B = -0.80
 C = -0.54
 D = -0.27
 E = 0.00
 F = 0.27

a) notch angle = 90°



A = -1.54
 B = -1.32
 C = -1.10
 D = -0.88
 E = -0.66
 F = -0.44
 G = -0.22
 H = 0.00
 I = 0.22

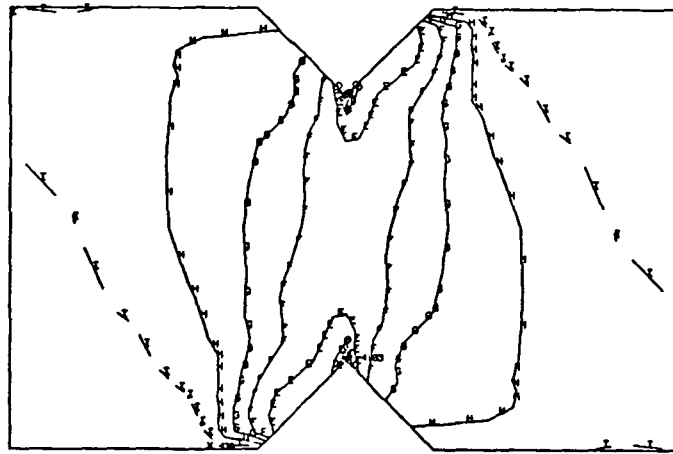
b) notch angle = 110°



A = -1.49
 B = -1.28
 C = -1.06
 D = -0.85
 E = -0.64
 F = -0.43
 G = -0.21
 H = 0.00
 I = 0.21

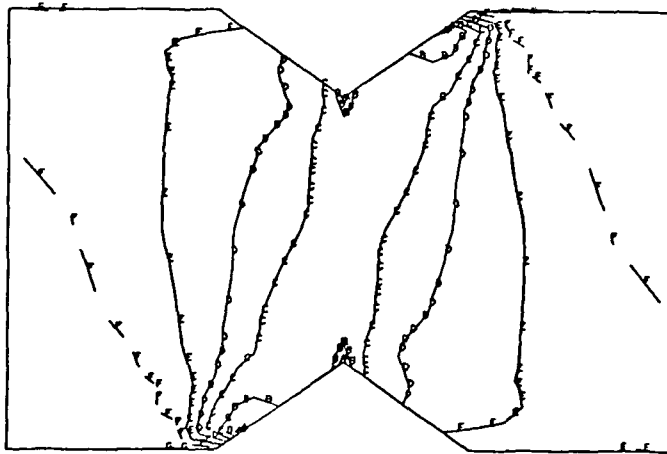
c) notch angle = 120°

Figure 39. Effect of Notch Angle on the Normalized Shear Stress Contours $\tau_{xy}/|\bar{\tau}|$ for an Orthotropy Ratio of 1.0; Notch Depth = 20 Percent, Notch Tip Radius = 0.00 mm.



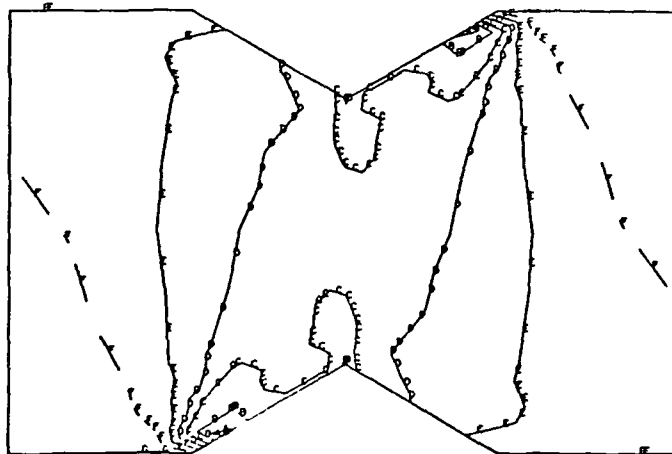
A = -1.94
 B = -1.69
 C = -1.45
 D = -1.21
 E = -0.97
 F = -0.73
 G = -0.48
 H = -0.24
 I = 0.00

a) notch angle = 90°



A = -1.37
 B = -1.10
 C = -0.82
 D = -0.55
 E = -0.27
 F = 0.00

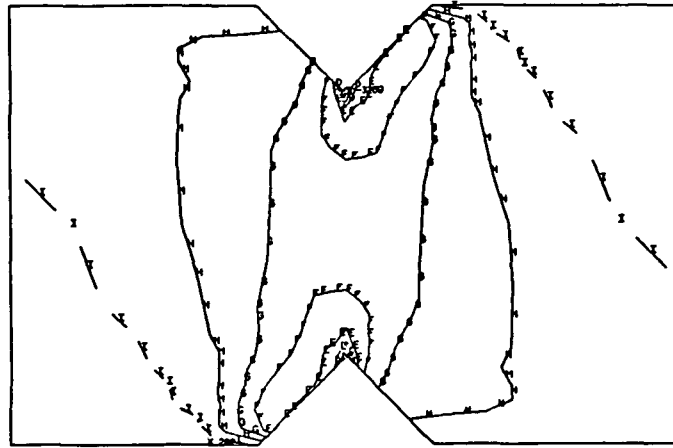
b) notch angle = 110°



A = -1.59
 B = -1.27
 C = -0.95
 D = -0.64
 E = -0.32
 F = 0.00
 G = 0.32

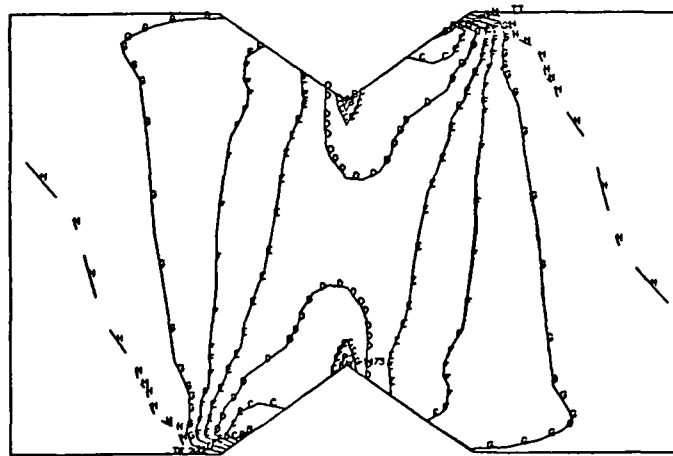
c) notch angle = 120°

Figure 40. Effect of Notch Angle on the Normalized Shear Stress Contours $\tau_{xy}/|\bar{\tau}|$ for an Orthotropy Ratio of 13.3; Notch Depth = 20 Percent, Notch Tip Radius = 0.00 mm.



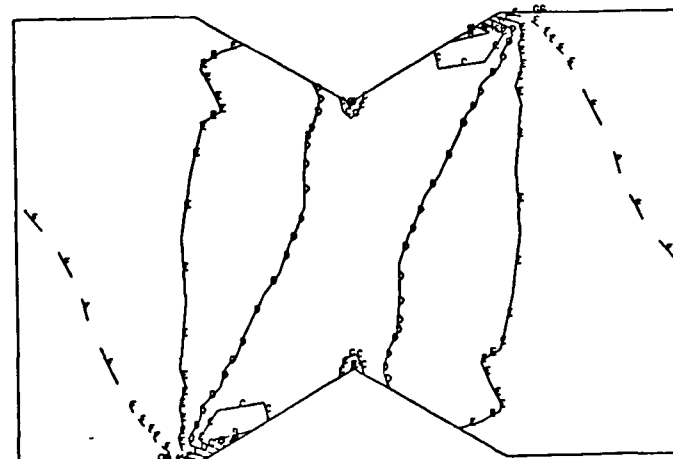
A = -2.32
 B = -2.03
 C = -1.74
 D = -1.45
 E = -1.16
 F = -0.87
 G = -0.58
 H = -0.29
 I = 0.00

a) notch angle = 90°



A = -1.56
 B = -1.33
 C = -1.11
 D = -0.89
 E = -0.67
 F = -0.44
 G = -0.22
 H = 0.00

b) notch angle = 110°



A = -1.94
 B = -1.55
 C = -1.16
 D = -0.78
 E = -0.39
 F = 0.00

c) notch angle = 120°

Figure 41. Effect of Notch Angle on the Normalized Shear Stress Contours $\tau_{xy}/|\bar{\tau}|$ for an Orthotropy Ratio of 49.4; Notch Depth = 20 Percent, Notch Tip Radius = 0.00 mm.

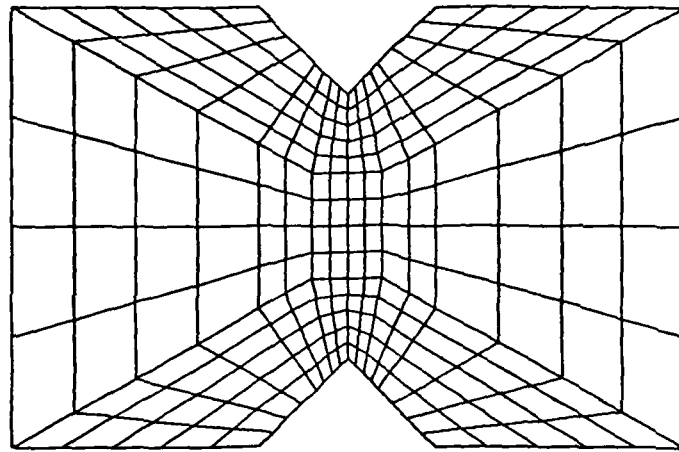
shown in Figures 40b and 40c, and 41b and 41c. The stress concentration at the notch root is a stronger function of notch tip radius than notch angle.

3.6 Effect of Notch Tip Radius

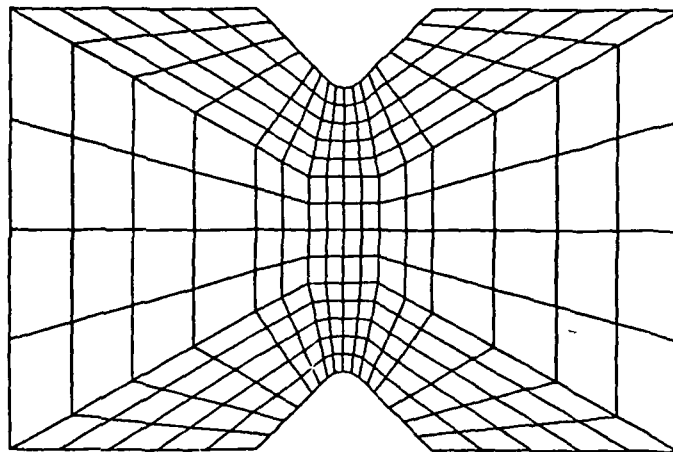
As has been previously discussed, the notches are present in the Iosipescu shear specimen to alter the shear stress distribution from parabolic to a more uniform distribution. There is no stress concentration of normal stresses; therefore it is reasonable to maintain the notch shape down to as narrow a region as possible, i.e., as small a notch tip radius as possible. Marloff arrived at the same conclusion when analyzing a similarly shaped test specimen [36]. However, the sharp notch (tip radius = 0.00 mm) does produce a shear stress concentration at the notch tip. Therefore, during this study, three different notch tip radii were modeled, in an attempt to establish a notch tip radius which will minimize this shear stress concentration. The finite element grids for these three geometries are shown in Figure 42.

Normalized shear stress profiles as a function of notch tip radius for all three materials are plotted in Figures 43 through 45. The larger notch tip radii definitely reduce the shear stress concentration for all three materials. The peak shear stress tends to decrease with increasing notch radius. The shear stress distributions within the orthotropic materials (see Figures 44 and 45) are still far from the desired uniform shear stress distribution. Shear stress still tends to rise near the notch tip.

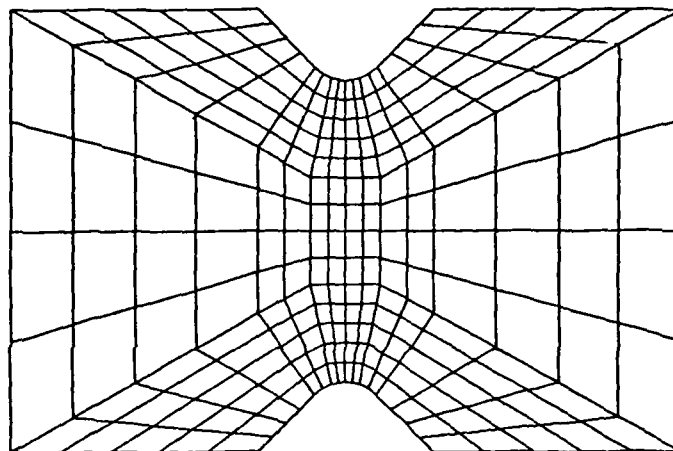
As would be expected, the shear stress gradients around the notch tips are also reduced with larger notch tip radii. This can be seen in



a) notch tip radius = 0.00 mm



b) notch tip radius = 0.64 mm

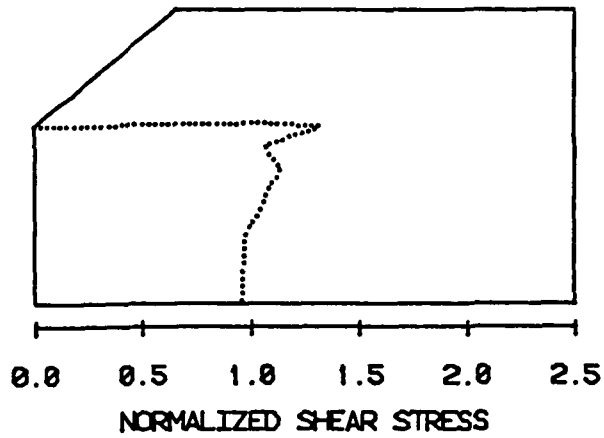


c) notch tip radius = 1.27 mm

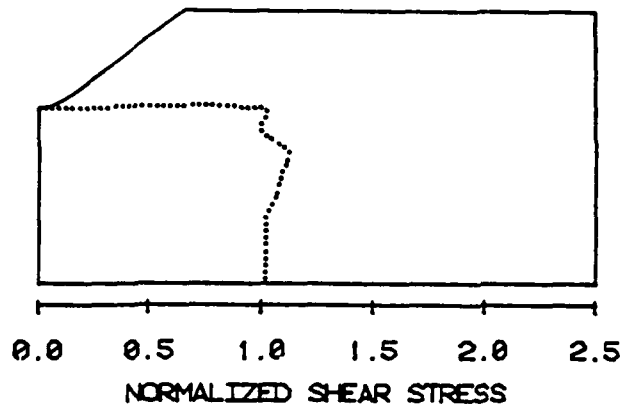
Figure 42. Finite Element Grids Used to Model Different Notch Tip Radii; Notch Depth = 20 Percent, Notch Angle = 90° .

CENTERLINE SHEAR STRESS DISTRIBUTION

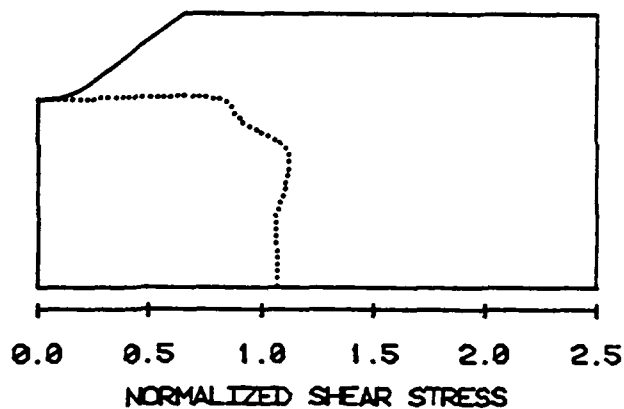
$E_{11}/E_{22} = 1.0$



a) notch tip radius = 0.00 mm



b) notch tip radius = 0.64 mm



c) notch tip radius = 1.27 mm

Figure 43. Effect of Notch Tip Radius on the Normalized Shear Stress Distribution $\tau_{xy}/\bar{\tau}$ Across the Notches for an Orthotropy Ratio of 1.0; Notch Depth = 20 Percent, Notch Angle = 90°.

CENTERLINE SHEAR STRESS DISTRIBUTION
 $E_{11}/E_{22} = 13.3$

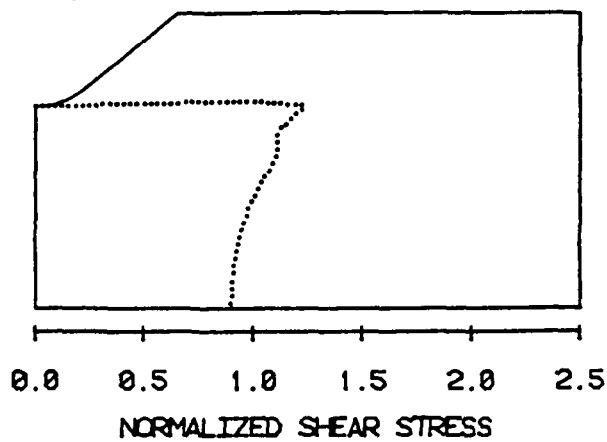
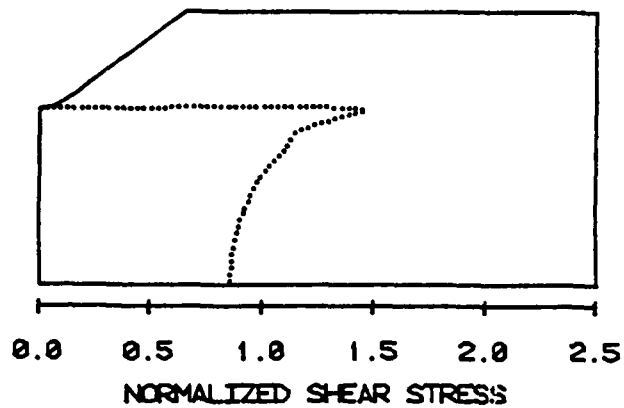
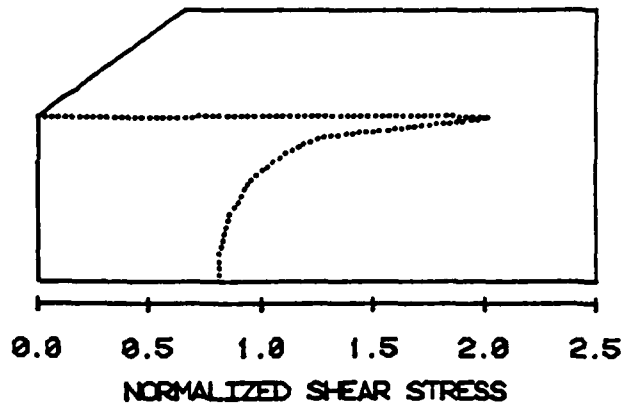
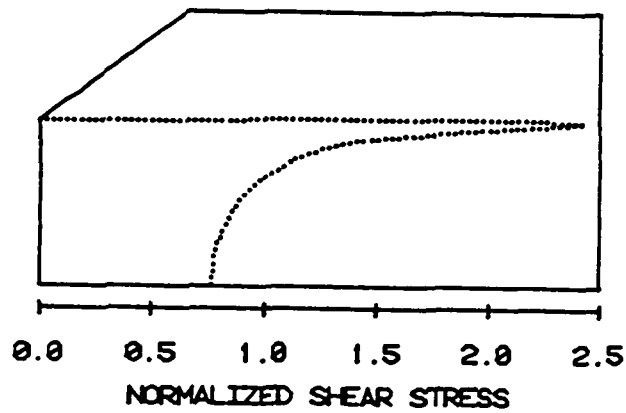
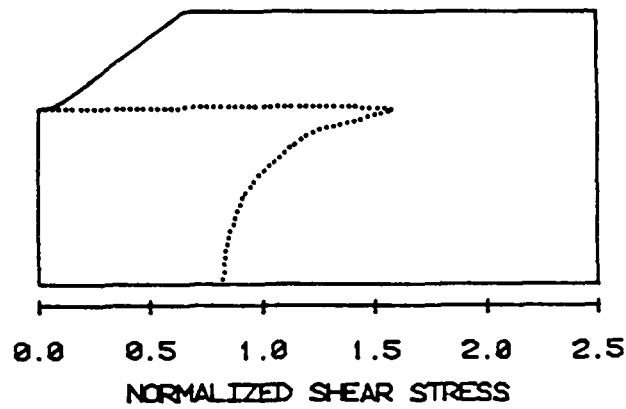


Figure 44. Effect of Notch Tip Radius on the Normalized Shear Stress Distribution $\tau_{xy}/\bar{\tau}$ Across the Notches for an Orthotropy Ratio of 13.3; Notch Depth = 20 Percent, Notch Angle = 90° .

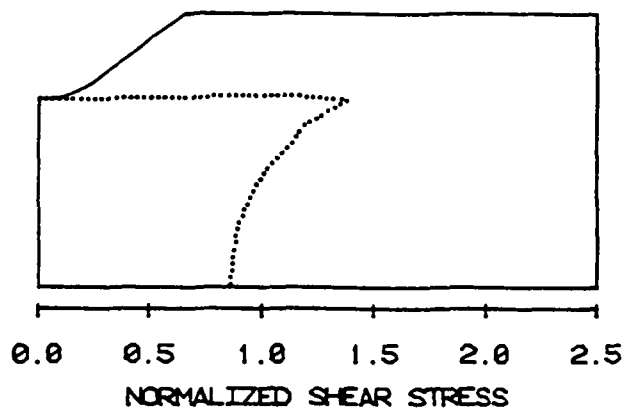
CENTERLINE SHEAR STRESS DISTRIBUTION
 $E_{11}/E_{22} = 49.4$



a) radius = 0.00 mm



b) radius = 0.64 mm



c) radius = 1.27 mm

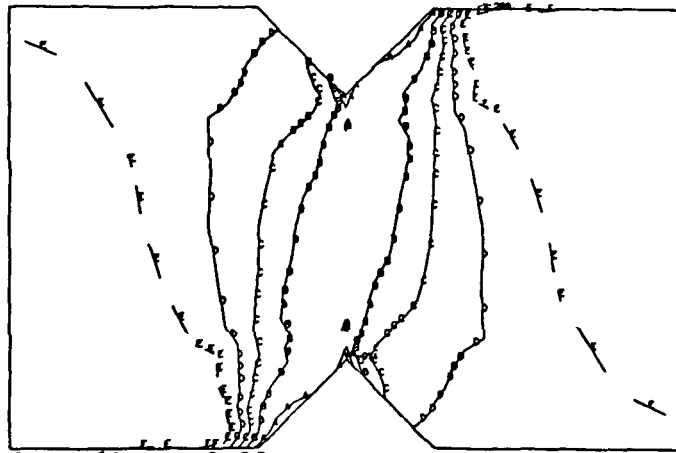
Figure 45. Effect of Notch Tip Radius on the Normalized Shear Stress Distribution $\tau_{xy}/\bar{\tau}$ Across the Notches for an Orthotropy Ratio of 49.4; Notch Depth = 20 Percent, Notch Angle = 90° .

the normalized shear stress contour plots shown in Figures 46 through 48. The point of maximum shear stress tends to move away from the centerline of the specimen for increasing notch tip radius. For the upper notch, the maximum shear stress has shifted to the right by approximately one notch radius in Figures 46c, 47c, and 48c when compared to the zero notch radius plots shown in Figures 46a, 47a, and 48a. Similar results were obtained by Marloff in his finite element study [36].

3.7 Optimum Specimen Geometry

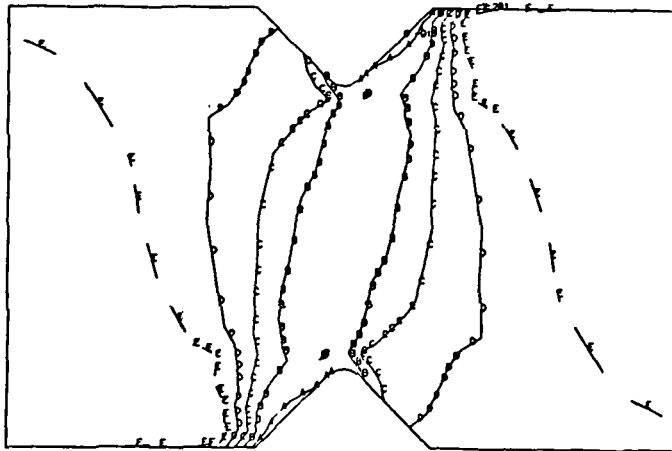
The Iosipescu shear test works well for isotropic materials, as can be seen from the previously presented shear stress distribution plots. The challenge is in developing this test method for use in measuring the shear properties, i.e., strength and stiffness, for highly orthotropic materials, particularly composite materials. Several trends have become evident in the present study. First of all, notch depth does not radically alter the shear stress distributions for any of the three materials analyzed. Second, the shear stress distribution is more favorably uniform for notch angles greater than 90° . Finally, the notch tip radius has a significant effect on the shear stress concentration produced by the notch.

In light of these observations, the finite element analysis was then run for the two orthotropic materials using the 20 percent notch depth, 120° notch angle, and the 1.27 mm (0.050 in) notch tip radius. Normalized shear stress distributions for these two cases are plotted in Figures 49 and 50. The shear stress distribution for the 13.3 orthotropy ratio material is about as uniform as might be achieved. The slight irregularities in the plot could easily be due to the coarseness



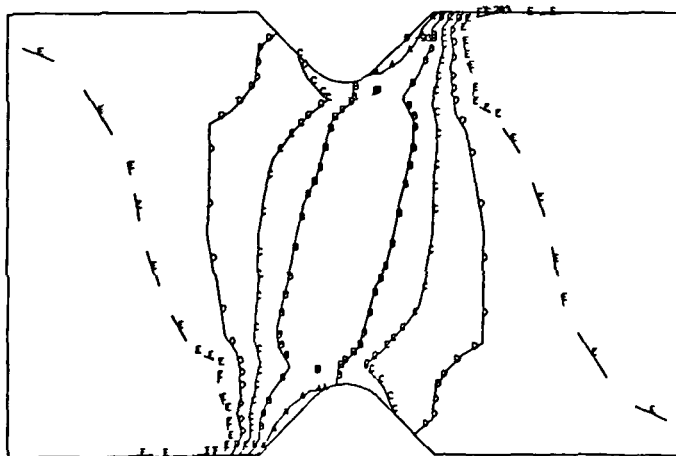
A = -1.07
 B = -0.80
 C = -0.54
 D = -0.27
 E = 0.00
 F = 0.27

a) notch tip radius = 0.00 mm



A = -1.14
 B = -0.85
 C = -0.57
 D = -0.28
 E = 0.00
 F = 0.28

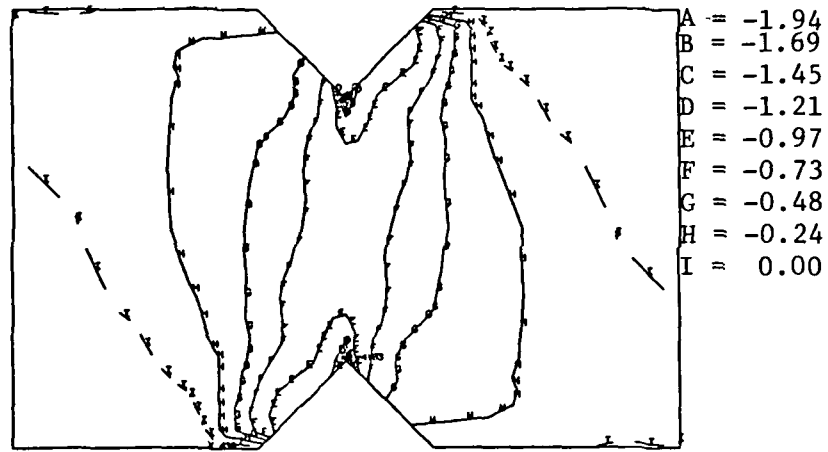
b) notch tip radius = 0.64 mm



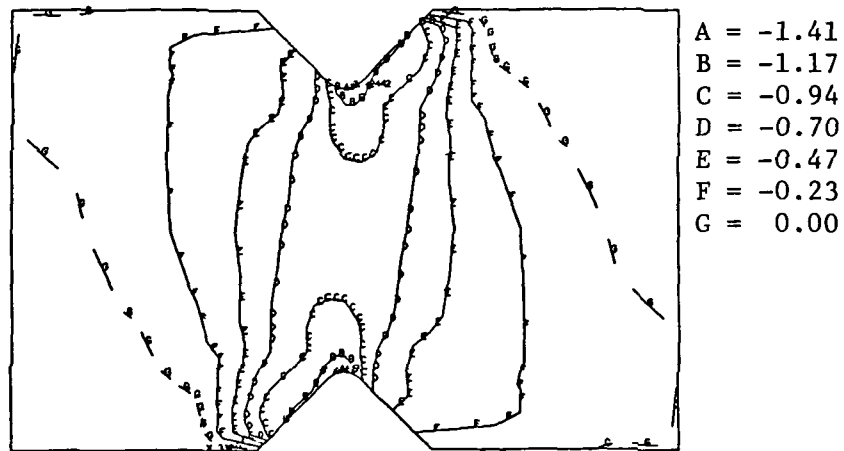
A = -1.21
 B = -0.91
 C = -0.61
 D = -0.30
 E = 0.00

c) notch tip radius = 1.27 mm

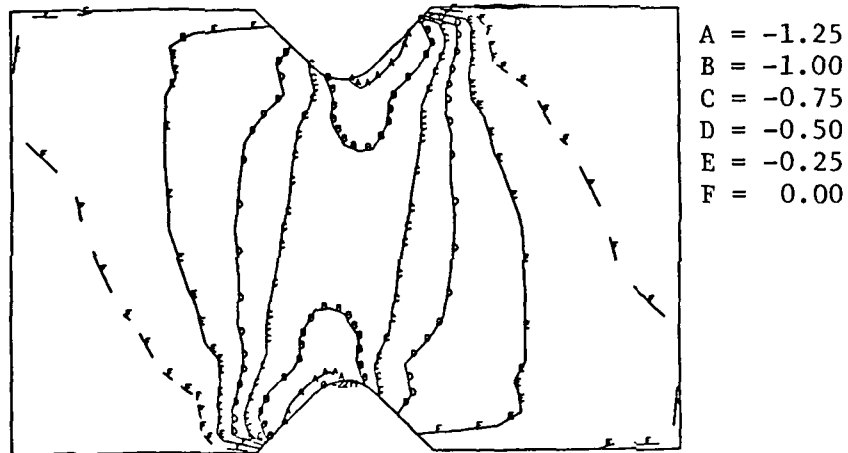
Figure 46. Effect of Notch Tip Radius on the Normalized Shear Stress Contours $\tau_{xy}/|\bar{\tau}|$ for an Orthotropy Ratio of 1.0; Notch Depth = 20 Percent, Notch Angle = 90° .



a) notch tip radius = 0.00 mm

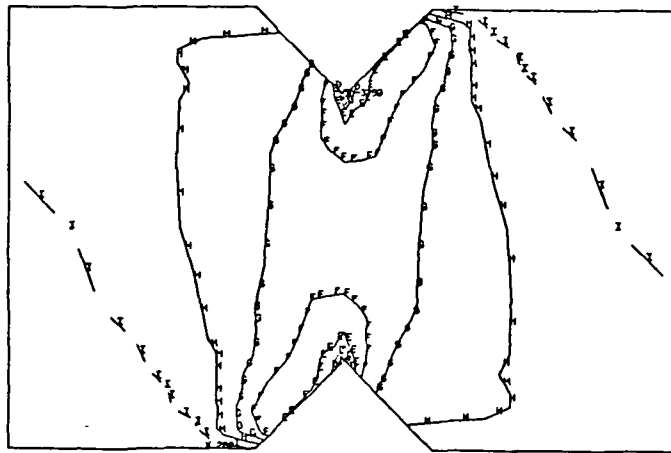


b) notch tip radius = 0.64 mm



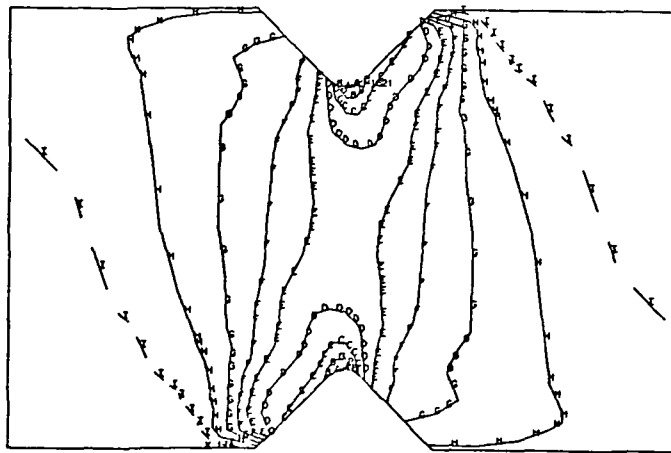
c) notch tip radius = 1.27 mm

Figure 47. Effect of Notch Tip Radius on the Normalized Shear Stress Contours $\tau_{xy}/|\bar{\tau}|$ for an Orthotropy Ratio of 13.3; Notch Depth = 20 Percent, Notch Angle = 90° .



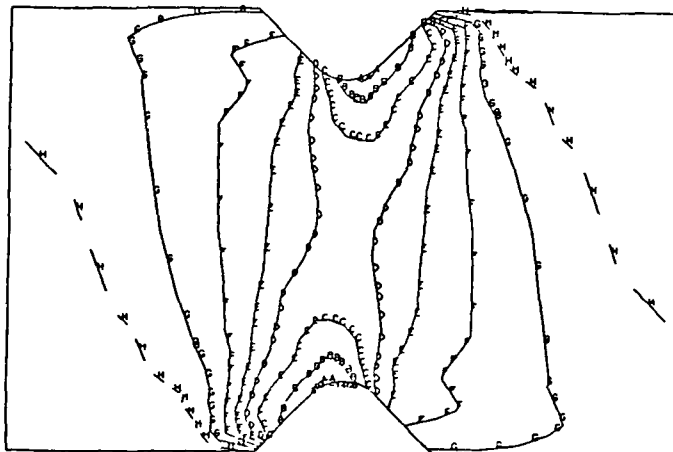
A = -2.32
 B = -2.03
 C = -1.74
 D = -1.45
 E = -1.16
 F = -0.87
 G = -0.58
 H = -0.29
 I = 0.00

a) notch tip radius = 0.00 mm



A = -1.54
 B = -1.34
 C = -1.15
 D = -0.96
 E = -0.77
 F = -0.58
 G = -0.38
 H = 0.19
 I = 0.00

b) notch tip radius = 0.64 mm



A = -1.42
 B = -1.22
 C = -1.02
 D = -0.82
 E = -0.61
 F = -0.41
 G = -0.20
 H = 0.00

c) notch tip radius = 1.27 mm

Figure 48. Effect of Notch Tip Radius on the Normalized Shear Stress Contours $\tau_{xy}/|\bar{\tau}|$ for an Orthotropy Ratio of 49.4; Notch Depth = 20 Percent, Notch Angle = 90° .

CENTERLINE SHEAR STRESS DISTRIBUTION

$$E_{11}/E_{22} = 13.3$$

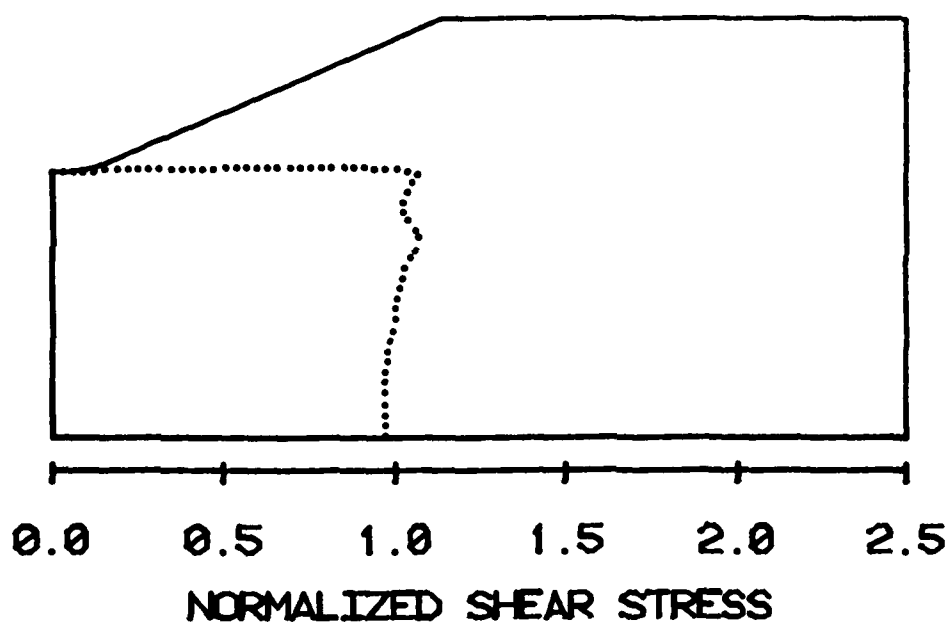


Figure 49. Normalized Shear Stress Distribution $\tau_{xy}/\bar{\tau}$ Across the Notches for an Orthotropy Ratio of 13.3; Notch Depth = 20 Percent, Notch Angle = 120° , Notch Tip Radius = 1.27 mm (0.050 in).

CENTERLINE SHEAR STRESS DISTRIBUTION

$$E_{11}/E_{22} = 49.4$$

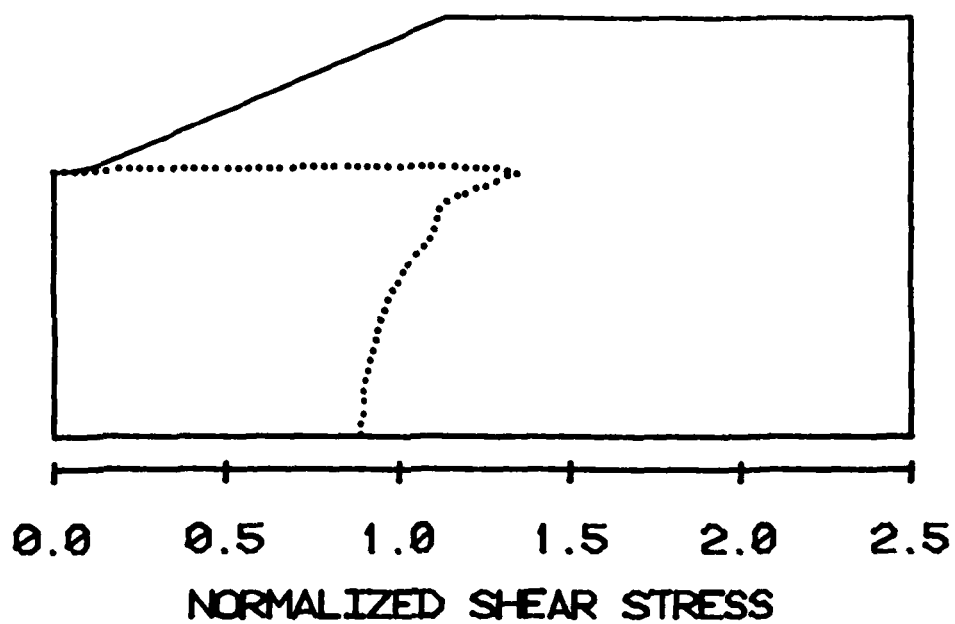


Figure 50. Normalized Shear Stress Distribution $\tau_{xy}/\bar{\tau}$ Across the Notches for an Orthotropy Ratio of 49.4; Notch Depth = 20 Percent, Notch Angle = 120° , Notch Tip Radius = 1.27 mm (0.050 in).

of the finite element grid used. The shear modulus calculated based on applied load and the strain within the instrumented area is in error by only 4.5 percent when compared to the input shear modulus.

The shear distribution for the 49.4 orthotropy ratio material shown in Figure 50 is not as uniform as the lower orthotropy ratio material shown in Figure 49. This difficulty in achieving a uniform shear stress distribution serves to point out the difficulty in testing highly orthotropic materials. However, one may still be able to measure shear properties of such highly orthotropic materials by testing $[0/90]_s$ layups. The shear properties remain unchanged, but the effective laminate orthotropy ratio is reduced. Iosepescu shear tests of laminates may induce significant interlaminar stress states, however, due to edge effects, particularly at the tip of the notch. These types of problems will be explored further in the second-year program.

Normalized shear stress contours in the notch region are plotted for each of the orthotropic materials, in Figures 51 and 52 respectively. The shear stress distribution is reasonably uniform and free of sharp stress gradients in the notch region, especially when compared to similar plots presented earlier.

Overall, the 20 percent notch depth, 120° notch angle, 127 mm (0.050 in) notch tip radius Iosipescu shear test specimen looks very favorable. This test specimen will be more extensively evaluated, both analytically and experimentally, during the second year of this program.

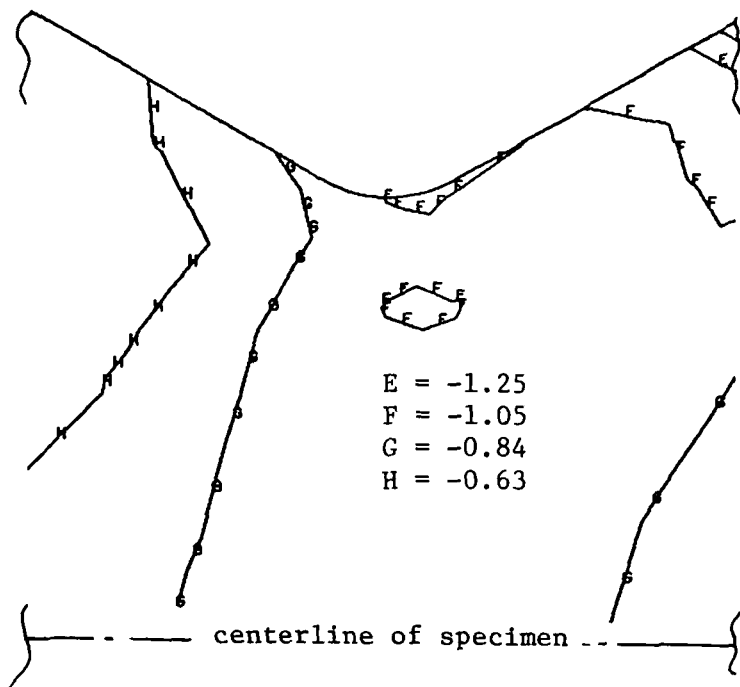


Figure 51. Normalized Shear Stress Contours $\tau_{xy}/|\bar{\tau}|$ in the Notch Region for an Orthotropy Ratio of 13.3; Notch Depth = 20 Percent, Notch Angle = 120° , Notch Tip Radius = 1.27 mm (0.05 in).

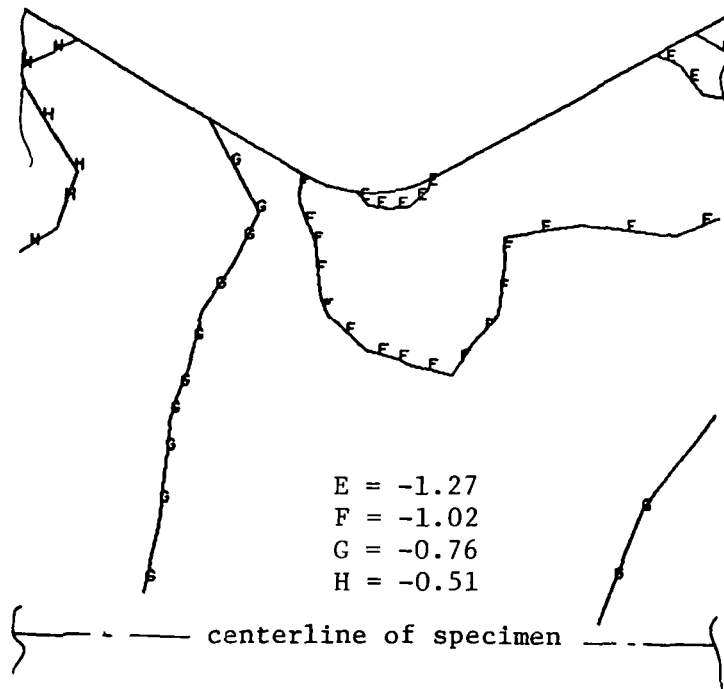


Figure 52. Normalized Shear Stress Contours $\tau_{xy}/|\bar{\tau}|$ in the Notch Region for an Orthotropy Ratio of 49.4; Notch Depth = 20 Percent, Notch Angle = 120° , Notch Tip Radius = 1.27 mm (0.05 in).

SECTION 4

TEST FIXTURE IMPROVEMENTS

4.1 Weaknesses of the Current Test Fixture

The present Wyoming version of the Iosipescu Shear Test has been used to measure shear properties of many different materials during the past six years. This version of the test fixture is now being used by other groups around the country as well. While the present fixture configuration, previously shown in Figure 3, works fairly well, several weaknesses in the design have become apparent. First of all, each side of the fixture is rigid, relying on a close fitting specimen in order to prevent rotation of the specimen during a test. Typically, all Iosipescu shear specimens fabricated by the CMRG at Wyoming are ground to width. This, of course, adds considerable time and expense to specimen fabrication. This problem can be solved by designing a fixture half which will clamp the specimen. The solution is not, however, to separate the fixture halves top-to-bottom. As previously discussed, when fixture halves are separated top-to-bottom rather than left-to-right, the loading point locations must be known. Therefore, cylindrical loading points are typically used, resulting in crushing of the specimen edges. This has been discussed in more detail in References [27,30].

A second weakness in the present fixture is the proximity of the loading points to the notch regions, as illustrated in Figure 2. As was discussed in Section 3, compressive stresses introduced at these close loading points intrude into the test region of the specimen. Any future redesign of the fixture will include moving these loading points back

from the notch area.

Other minor weaknesses of the present design include the small access area present for instrumentation of a test specimen. This small area also makes specimen installation somewhat clumsy, slowing testing. Finally, problems have been encountered with sticking of the sliding bearings during subambient or elevated temperature testing, particularly when fatigue testing, due to thickening or loss of the lubricant.

Overall, the weaknesses, with the exception of the loading point location, are minor. All four listed weaknesses are easily remedied.

4.2 Redesigned Test Fixture

A conceptual drawing of a possible future generation Iosipescu shear test fixture is shown in Figure 53. As can be seen in comparing Figure 53 with Figure 2, the loading points nearest the notches have been moved away from the center of the test specimen. This should eliminate the problem of compressive stresses introduced by the loading

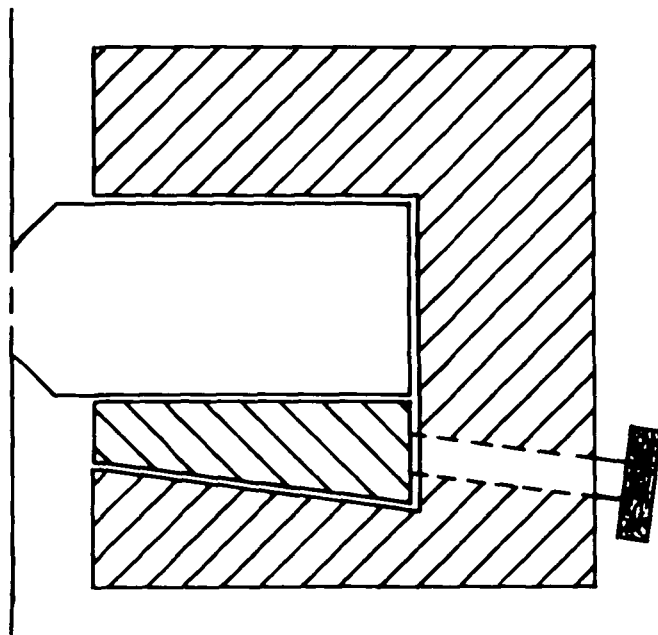


Figure 53. Conceptual Drawing of a Clamping Iosipescu Shear Test Fixture Half.

surface infringing on the test region. A clamping mechanism has been added to ensure a tight fit between specimen and fixture, preventing any rotation of the specimen during the test. The wedge design is a very rigid mechanism, assuring uniform clamping force throughout a test, without the need for excessively large clamping forces.

Greater access will be provided in the new fixture for installation and observation of strain instrumentation. Also, roller bearings may be used to eliminate the sticking problem sometimes encountered during nonambient temperature fatigue tests. Or perhaps the fixture may be designed such that the separate halves are attached only to the testing machine. This would eliminate the need for bearings.

This test fixture design will be completed during the second year of this program. A fixture will be built and experimentally tested to verify that the fixture operates correctly.

SECTION 5
DISCUSSION

The goal of this research program was to analytically model the stress state within an Iosipescu shear test specimen. Once the stress state was understood, the specimen and test fixture could be modified in order to achieve an optimized shear test method for orthotropic materials. In order to accomplish this program, nine different finite element models of the Iosipescu Shear Test specimen were constructed. These models were analyzed using material properties for three different degrees of orthotropy, ranging from 1 to 49. The resulting stress distributions were studied and the following changes in the test method are proposed:

- 1) The loading points nearest the notches in the Iosipescu shear specimen should be moved away from the center of the test specimen.
- 2) The notch geometry should be modified to include a larger notch tip radius and a larger notch angle.

The test fixture should also be redesigned to accomplish the following:

- 1) A clamping mechanism could be designed to minimize specimen rotation during testing. This will permit the relaxation of the strict tolerances on specimen width currently required, resulting in a lower fabrication cost per specimen.
- 2) Roller bearings or perhaps totally separate fixture halves could be used to eliminate binding during nonambient temperature tests.

- 3) A larger window for strain instrumentation should be included, to allow for easier installation of the specimen into the fixture.

The second year of this research study on the design and application of the Iosipescu Shear Test will include further finite element modeling of the test specimen geometry. True three-dimensional geometries will be examined, to identify potential problems due to edge effects or other three-dimensional stress problems at the notch tip. An elastoplastic orthotropic analysis will be used. Actual laminates composed of discrete plies will be studied, as opposed to two-dimensional models with smeared properties.

Test fixture redesign will be performed and a new test fixture built. This will be used to verify the stress state within the test specimen by Moire' interferometry and/or photoelasticity. Sufficient shear tests will be conducted on materials of known properties to provide a statistically valid verification of the fixture performance. This experimental effort will complement an in-house study of various shear test methods, this study being performed to establish the best available method for measuring shear properties of orthotropic materials.

A secondary task within the second-year program will be to examine the possibility of designing an external transducer to measure shear strains. This device will be similar in function to an extensometer used in tensile tests. The CMRG at Wyoming has previously experimented with such a device [30] but further work needs to be done. This device would replace the strain gages currently used to measure shear strains. Strain gages work well for ambient environment tests, but are difficult

to use when testing polymer matrix composites at elevated temperatures. The total shear strain range of the strain gages is also limited.

Finally, a series of Iosipescu shear tests will be conducted to measure the shear properties of several different composite material systems, in order to provide useful design data. The actual test matrix will be defined during the follow-on program.

REFERENCES

1. N. J. Pagano and J. M. Whitney, "Geometric Design of Composite Cylindrical Characterization Specimens," Journal of Composite Materials, Vol. 4, October 1970, pp. 538-548.
2. A. Feldman, J. Tasi, and D. A. Stany, "Experimental Determination of Stiffness Properties of Thin-Shell Composite Cylinders," Experimental Mechanics, Vol. 8, 1966, pp. 385-394.
3. D. F. Adams and R. L. Thomas, "The Solid-Rod Torsion Test for the Determination of Unidirectional Composite Shear Properties," Textile Research Journal, Vol. 39, No. 4, April 1969, pp. 339-345.
4. C. C. Chamis and J. H. Sinclair, "10⁰ Off-Axis Tensile Test for Intra-laminar Shear Characterization of Fiber Composites," NASA Technical Note No. NASA TN D-8215, April 1976.
5. B. W. Rosen, "A Simple Procedure for Experimental Determination of the Longitudinal Shear Modulus of Unidirectional Composites," Journal of Composite Materials, Vol. 6, October 1972, pp. 552-554.
6. D. F. Sims, "In-Plane Shear Stress-Strain Response of Unidirectional Composite Materials," Journal of Composite Materials, Vol. 7, January 1973, pp. 124-128.
7. H. T. Hahn, "A Note on Determination of the Shear Stress-Strain Response of Unidirectional Composites," Journal of Composite Materials, Vol. 7, July 1973, pp. 383-386.
8. E. L. Bryan, "Photoelastic Investigation of Stress Distribution in the Panel Shear Specimen," Symposium for Torsion Shear Testing, ASTM STP 289, 1961, pp. 90-94.
9. R. N. Hadcock and J. B. Whiteside, "Characterization of Anisotropic Composite Materials," Composite Materials: Testing and Design, ASTM STP 460, 1969, pp. 37-47.
10. J. M. Whitney, D. L. Stansbarger, and H. B. Howell, "Analysis of the Rail Shear Test - Applications and Limitations," Journal of Composite Materials, Vol. 5, January 1971, pp. 24-34.
11. R. Garcia, T. A. Weisshaar, and R. R. McWithey, "An Experimental and Analytical Investigation of the Rail Shear-test Method as Applied to Composite Materials," Experimental Mechanics, Vol. 20, No. 8, August 1980, pp. 273-279.
12. G. L. Farley and D. J. Baker, "In-plane Shear Test of Thin Panels," Experimental Mechanics, Vol. 23, No. 1, March 1983, pp. 81-88.
13. M. E. Waddoups, "Characterization and Design of Composite Materials," Composite Materials Workshop, Technomic Publishing Co., Inc., Stanford, Connecticut, 1968.

14. P. H. Petit, "A Simplified Method of Determining In-plane Shear Stress-Strain Response of Unidirectional Composites," Composite Materials: Testing and Design, ASTM STP 460, 1969, pp. 83-93.
15. E. M. Lenoë, "Testing and Design of Advanced Composite Materials," Journal of the Engineering Mechanics Division A.S.C.E., Vol. 96, December 1970, pp. 809-823.
16. M. F. Duggan, "An Experimental Evaluation of the Slotted-tension Shear Test for Composite Materials," Experimental Mechanics, Vol. 20, No. 7, July 1980, pp. 233-239.
17. R. K. Witt, W. H. Hopman II, and R. S. Buxbaum, "Determination of Elastic Constants of Orthotropic Materials with Special Reference to Laminates," ASTM Bulletin No. 194, 1953, pp. 53-57.
18. S. W. Tsai, "Experimental Determination of the Elastic Behavior of Orthotropic Plates," Journal of Engineering for Industry, August 1965, pp. 315-318.
19. "Apparent Horizontal Shear Strength of Reinforced Plastics by Short Beam Method," ASTM D 2344-76, Part 36, 1979, pp. 374-377.
20. L. B. Greszczuk, "Shear Modulus Determination of Isotropic and Composite Materials," Composite Materials: Testing and Design, ASTM STP 460, 1969, pp. 140-149.
21. N. Iosipescu, "New Accurate Procedure for Single Shear Testing of Metals," Journal of Materials, Vol. 2, No. 3, September 1967, pp. 537-566.
22. D. E. Walrath and D. F. Adams, "Damage Mechanisms/Failure Mechanics of Carbon-Carbon Composite Materials," Report UWME-DR-904-101-1, Department of Mechanical Engineering, University of Wyoming, Laramie, Wyoming, September, 1979.
23. D. E. Walrath and D. F. Adams, "Test Methods Development for 3-D Cylindrical-Weave Carbon-Carbon Composite Materials," Report UWME-DR-104-104-1, Department of Mechanical Engineering, University of Wyoming, Laramie, Wyoming, September 1981.
24. D. E. Walrath and D. F. Adams, "Iosipescu Shear Tests to Study Effects of Variations in the Fiber/Matrix Interface of Graphite/Epoxy Composites," Report UWME-DR-004-108-1, Department of Mechanical Engineering, University of Wyoming, Laramie, Wyoming, November 1980.
25. D. E. Walrath and D. F. Adams, "Mechanical Properties of ISF-Toughened Graphite/Epoxy Composites," Report UWME-DR-104-103-1, Department of Mechanical Engineering, University of Wyoming, Laramie, Wyoming, June 1981.

26. S. J. Davis and D. F. Adams, "Thermal Deformation of Various Composite Material Ski Constructions," Report UWME-DR-101-103-1, Department of Mechanical Engineering, University of Wyoming, Laramie, Wyoming, May 1981.
27. D. F. Adams and D. E. Walrath, "Iosipescu Shear Properties of SMC Composite Materials", Composite Materials: Testing and Design (Sixth Conference), ASTM STP 787, 1982, pp. 19-33.
28. D. E. Walrath and D. F. Adams, "Shear Strength and Modulus of SMC-R50 and XMC-3 Composite Materials," Report UWME-DR-004-105-1, Department of Mechanical Engineering, University of Wyoming, Laramie, Wyoming, March 1980.
29. D. E. Walrath and D. F. Adams, "Static and Dynamic Shear Testing of SMC Composite Materials," Report UWME-DR-004-103-1, Department of Mechanical Engineering, University of Wyoming, Laramie, Wyoming, May 1980.
30. D. E. Walrath and D. F. Adams, "The Iosipescu Shear Test as Applied to Composite materials," Experimental Mechanics, Vol. 23, No. 1, March 1983, pp. 105-110.
31. J. M. Slepetz, T. F. Zagaeski, and R. F. Novello, "In-plane Shear Test For Composite Materials," Report No. AMMRC TR 78-30, Army Materials and Mechanics Research Center, Watertown, Massachusetts, July 1978.
32. M. Arcan, Z. Hashin, and A. Voloshin, "A Method to Produce Uniform Plane-stress States with Applications to Fiber-reinforced Materials," Experimental Mechanics, Vol. 18, No. 4, 1978, pp. 141-146.
33. A. Voloshin and L. Arcan, "Failure of Glass/Epoxy Lamina - Fractographic Study," Journal of Composite Materials, Vol. 13, No. 3, July 1979, pp. 240-246.
34. A. Voloshin and M. Arcan, "Failure of Unidirectional Fiber-Reinforced Materials - New Methodology and Results," Experimental Mechanics, Vol. 20, No. 8, August 1980, pp. 280-284.
35. A. Voloshin and M. Arcan, "Pure Shear Moduli of Unidirectional Fibre Reinforced Materials (FRM)", Fibre Science and Technology, Vol. 13, No. 2, March-April 1980, pp. 125-134.
36. R. H. Marloff, "Finite Element Analysis of Biaxial Stress Test Specimen for Graphite/Epoxy and Glass Fabric/Epoxy Composites," Composite Materials: Testing and Design (Sixth Conference), ASTM STP 787, 1982, pp. 34-49.
37. H. W. Bergner, Jr., J. G. Davis, Jr., and C. T. Herakovich, "Analysis of Shear Test Method for Composite Laminates," Report VPI-E-77-14, Virginia Polytechnic Institute and State University, Blacksburg, Virginia, April 1977.

38. C. T. Herakovich and H. W. Bergner, Jr., "Finite Element Stress Analysis of a Notched Coupon Specimen for In-plane Shear Behavior of Composites," Composites, July 1980, pp. 149-154.
39. Metals Handbook, Volume 2 - Properties and Selection: Nonferrous Alloys and Pure Metals, Ninth Edition, American Society for Metals, 1979.
40. Military Handbook 5A, "Metallic Materials and Elements for Aerospace Vehicle Structures," Department of Defense, Washington, DC, 1966.
41. "Advanced Composites Design Guide, Vol. IV - Materials," Third Edition, Air Force Flight Dynamics Laboratory, Dayton, Ohio, (Third Revision) January 1977.